Discriminating Noise from Chaos in Heart Rate Variability:

Application to Prognosis in Heart Failure

by

Natalia M. Arzeno

S.B. Electrical Science and Engineering
Massachusetts Institute of Technology, 2006

Submitted to the Department of Electrical Engineering and Computer Science

in Partial Fulfillment of the Requirements for the Degree of

Master of Engineering in Electrical Engineering and Computer Science

at the Massachusetts Institute of Technology

May 2007
[June 2007]

Author_____
Department of Electrical Engineering and Computer Science
May 25, 2007

Certified by_____
Chi-Sang Poon
arch Scientist
sis Supervisor

Accepted by_____
thur C. Smith
l Engineering
Chairman, Department Committee on Graduate Theses

Discriminating Noise from Chaos in Heart Rate Variability:

Application to Prognosis in Heart Failure

by

Natalia M. Arzeno

Submitted to the
Department of Electrical Engineering and Computer Science

May 25, 2007

In Partial Fulfillment of the Requirements for the Degree of
Master of Engineering in Electrical Engineering and Computer Science

ABSTRACT

This thesis examines two challenging problems in chaos analysis: distinguishing deterministic chaos and stochastic (noise-induced) chaos, and applying chaotic heart rate variability (HRV) analysis to the prognosis of mortality in congestive heart failure (CHF).

Distinguishing noise from chaos poses a major challenge in nonlinear dynamics theory since the addition of dynamic noise can make a non-chaotic nonlinear system exhibit stochastic chaos, a concept which is not well-defined and is the center of heated debate in chaos theory. A novel method for detecting dynamic noise in chaotic series is proposed in Part I of this thesis.

In Part II, we show that linear and nonlinear analyses of HRV yield independent predictors of mortality. Specifically, sudden death is best predicted by frequency analysis whereas nonlinear and chaos indices are more selective for progressive pump failure death. These findings suggest a novel noninvasive probe for the clinical management of CHF patients.

Thesis Supervisor: Chi-Sang Poon
Title: Principal Research Scientist

Table of Contents

List of Figures

List of Tables

Introduction

Chaos analysis has presented countless challenges from the full understanding of the seemingly random, yet deterministic, systems to detection of chaotic dynamics in experimental data, to the application of chaotic system properties in the real world. Many have proposed solutions to these challenges, but the full potential of chaotic system analysis is yet to be discovered. Two remaining challenges in chaos analysis are discussed in this thesis: identifying noise as stochastic or deterministic in chaotic series, and determining the risk of death of patients with congestive heart failure (CHF) from the chaotic heart rate series.

The detection of chaos in noisy signals has been approached in various manners [1-3]. Similarly, the effect of noise on chaotic signals and noise-induced chaos have been previously explored [4-6]. However, only one group has approached the identification of the type of noise in chaotic signals [7], an interesting problem since noise identification can lead into further understanding of the underlying system dynamics. Strumik *et. al.* [7] found dynamic noise in the Hénon and Ikeda maps could be represented as measurement "pseudonoise" of the Cauchy distribution and designed an algorithm based on correlation entropy for noise identification which, though reliable for dynamic noise, was not reliable for measurement noise. The algorithm in [7] is also limited by the lack of systems for testing, thus a new noise identification algorithm is essential. The first part of the thesis introduces an algorithm which identifies if well-known chaotic maps are contaminated with additive dynamic noise —resulting from noise that affects the future chaotic dynamics at each time point— or deterministic measurement noise— where the noise is superimposed on the chaotic dynamics— mimicking the effect of a measuring device. Chapter 1 focuses on chaos theory: the definition of chaos, the ways chaos can be achieved and the effect of noise on chaotic systems. In addition, various physiological systems that exhibit chaotic dynamics are explained in the chapter. The second part of Chapter 1 defines the chaos maps used for the analysis— logistic, Hénon, Ikeda, Lorenz, and Mackey-Glass—as well as their previous applications or realizations in nature. The nonlinear modeling and chaos detection theory are described in Chapter 2. Chapter 3 delves into the choice of parameters for the chaos maps and the effect of dynamic and measurement noise on the logistic and Hénon maps. The approach to system noise identification by means of Volterra series approximations and the parameters used in the simulations are described in Chapter 4. Chapter 5 states

the results and limitations of the study, where improvements and alternate algorithms are suggested in the last section of the chapter.

Congestive heart failure, the inability of the heart to pump enough blood to the body, is the common end of various diseases such as coronary artery disease and congenital heart disease. Two kinds of death commonly accompany CHF: sudden cardiac death and death from progressive pump failure. Pump failure death often occurs after progressive worsening of the CHF symptoms whereas sudden death implies a fatal electrical event (arrhythmic event) taking place during a time of clinical stability and is typically a manifestation of reduced left ventricular function [8, 9]. Heart rate variability (HRV) analysis in the congestive heart failure population has become of interest over the past decade as a predictor for specific kinds of death in CHF. Linear and nonlinear analysis of HRV provides a non-invasive, inexpensive method to detect autonomic changes and aid the physician's treatment of the condition. Results of previous studies rely heavily on the advancement of the disease in the subject group as well as the number of subjects included in the study such that studies often present contradictory results [10]. In addition, previous studies typically focus on a subset of HRV indices, analyzing traditional time- and frequency-domain parameters in combination with either complexity or nonlinear indices. The lack of a comprehensive set of HRV indices in a single study prevents the identification of independent predictors of mortality. The second part of the thesis focuses on combining several traditional linear and less-applied nonlinear—including chaotic—indices of heart rate variability to determine the significant univariate and multivariate predictive factors of all-cause death, sudden death, and progressive pump failure death in patients with congestive heart failure. Chapter 6 characterizes congestive heart failure and heart rate variability. The physiological markers of CHF are discussed along with the different modes of death that accompany the disease. The use and significance of heart rate variability in a variety of situations is discussed, including previous works using HRV for risk stratification of mortality in CHF. The dataset is described in Chapter 7 along with the definition and calculation of the HRV indices used in the analysis. The results for the three types of survival analysis—receiver operating curve (ROC), support vector machine classification (SVC), and Cox proportional hazards—are stated in Chapters 8 and 9. Chapter 8 encompasses the ROC and SVC results from division of the data into a training set and a test set. The Cox hazards results for the training set are also stated for characterization and validation of the training set. The results for analysis of the complete data set are described in Chapter 9 for all-cause mortality, sudden

death, and death from progressive heart failure. Chapter 10 encompasses the analysis of the results, main contributions of the study, and future work.

Part I

Volterra Series Approach for Distinguishing Deterministic and Stochastic Noise in Chaotic Series

Chapter 1 Chaos Theory and Occurrence

Over the past decades, an interest in studying, defining, and characterizing chaotic series has emerged. The challenges of defining what specific properties are comprised in a chaotic series, how to define equations such that they mimic chaotic occurrences in nature, and how to detect the presence and level of chaos in a signal have been approached in different ways. In this chapter, the various sections explain the particular characteristics of chaotic series, the different ways chaos can be reached, the effect of noise on chaotic series, and several physiological systems which exhibit chaotic dynamics. Section 1 delves into the definition of chaos, the specific properties of the apparently random but deterministic dynamics in the time-domain and the phase-space, and introduces a relative measure of chaos intensity in noise-free systems. The equations that define chaotic dynamics only do so for certain parameters, where a slight change in the equation parameters can result in a periodic series. The most common routes to chaos through the variation of a specific parameter in the equation, as well as the topological properties that are implied by the routes to chaos, are described in Section 2. Chaotic dynamics in nature are often contaminated by noise. Section 3 presents various works on the effect of noise on chaotic series and introduces the controversy of "noise-induced chaos." Section 4 explores different occurrences of chaos in physiological systems, both in anatomical structures and reactions to particular stimuli. The chaos maps used in analyzing the noise identification algorithms are defined in Section 5.

1.1 What is chaos?

Chaotic series are often mistaken as randomness, when in reality they are deterministic nonlinear dynamical systems with great dependence on initial conditions. For example, two chaotic series described by the same equations but with slightly different initial conditions (e.g. difference of 10^{-6}) will have diverging trajectories. A series is classified as chaotic if it fulfills three conditions [11]:

1. it displays sensitivity to initial conditions
2. it is topologically transitive
3. its periodic orbits are dense

The sensitivity to initial conditions of a signal is quantified by the Lyapunov exponent. The Lyapunov exponent determines the presence and degree of chaos in noise-free systems and corresponds to the

average separation rate of neighboring trajectories. In a one-dimensional map the Lyapunov exponent is defined as [11]:

$$\lambda = \lim_{n\to\infty} \frac{1}{n} \sum_{i=0}^{n-1} \log \frac{|\partial x_{n+1}|}{|\partial x_n|} = \lim_{n\to\infty} \frac{1}{n} \sum_{i=0}^{n-1} \log \left| \frac{df}{dx}\left(f^i(x_0)\right) \right| \tag{1.1}$$

The Lyapunov exponent has been shown to be independent of initial conditions (x_0) and is positive for series with sensitivity to initial conditions.

Topological transitivity and topological mixing express the evolution of the series trajectories; although chaotic dynamics are deterministic, they are asymptotically unpredictable. The condition of dense periodic orbits requires any interval to contain infinite periodic orbits with high period. If the chaotic series is expansive—iterations of points in any given subinterval will eventually cover the entire interval after a sufficient number of iterations—then all three conditions for chaos are satisfied.

Chaotic dynamic in a system usually only cover a subset of the phase space, such that the chaotic behavior falls on an attractor. The attractor is defined by three properties: it is a closed invariant set, it attracts an open set of initial conditions, and it is minimal [12]. The stability of the trajectories depends on the convergence to the attractor (Poisson) and the convergence within the attractor (Lyapunov) [13]. If the attractor exhibits sensitivity to initial conditions, it is called a strange attractor [12]. Strange chaotic attractors are characterized by their complex geometrical structure, at least one positive Lyapunov exponent, and fractal (non-unity) dimension.

1.2 Routes to chaos

In dynamical systems, there are three major routes to chaos [13]:

1. period-doubling
2. intermittency
3. quasiperiodicity destruction

The period-doubling route to chaos is reached by a series of period-doubling bifurcations, , up to a critical parameter where there are infinite periods. Past the critical parameter, the system becomes unstable, according to Lyapunov, with aperiodic oscillations and exhibits chaotic properties. Maps which reach

chaos through the period-doubling route, such as the Hénon map, are characterized by a dimension between 2 and 3 and a strange attractor with a horseshoe shape [13]. The intermittency route to chaos is characterized by a sudden transition from regular oscillations to chaos. The phenomenon of intermittency occurs when chaotic dynamics are interspersed with periodic-like behavior soon after the critical parameter. In the course of intermittency, the structure of the phase space and the basin of attraction can be radically changed with a single bifurcation, resulting in a *crisis*. The final route to chaos, destruction of a quasiperiodic orbit occurs when a torus is destroyed in phase space such that the new trajectories have a fractal dimension [13]. The three routes to chaos have been previously shown in low- and high-dimensional systems, where all three routes can exist for the same dynamical system as characterized by exploring different regions and directions in the parameter space.

1.3 Noise and chaos

The effects of dynamic noise in chaotic series, both in additive and multiplicative form, have been previously studied in theory and applications. In the present study, the focus will be on dynamic noise of the additive form. Though several studies have agreed on the existence of noise-induced chaos, others [14] with stricter mathematical definitions argue noise affects the nonlinear properties of the series but its stochastic nature prevents the result from being defined as chaotic. Gassmann [6] studied the effect of stochastic noise in the time series to find a state of interest in a chaotic signal. He defined three regions of interest depending on the variance of the added noise, where the region with largest noise caused dramatic shortening of transients. Gao [4, 5] later focused on dynamic noise converting a highly periodic system to a system with chaos-like motions, where the chaos can arise from changing between two periodic states or between a periodic state and a metastable chaotic state. Like Gaussmann, Gao found three regions of different behavior such that certain noise intensities resulted in Brownian-like motion and others in chaotic-like motions. In addition to inducing chaos in a signal, additive dynamic noise can also stabilize stochastic oscillations, excite oscillations, and induce on-off intermittency and phase transitions, such that in a first-order transition a small change in the control parameter drastically changes the output [15].

The effects of additive measurement noise have not been well studied in chaotic signals since it does not contribute to the chaotic dynamics. The addition of noise to the clean signal, resulting in the observed series, prevents a periodic series from being kicked into the chaotic attractor. In addition, the

superposition of noise onto a chaotic series would only shadow the underlying dynamics rather than force the signal into a different regime.

1.4 Chaos in biological systems

Chaos characterizes numerous biological and physiological systems both in health and disease state. Anatomical structures, such as the His-Purkinje system, chordae tendineae, the vascular tree, and the lung tree contain fractal properties [16]. Many studies over the past decades have concentrated on cardiac [16-20] and neural [17, 20-22] chaos, analyzing the change in chaotic dynamics for a variety of stimuli and subjects with different pathologies, as well as controlling harmful chaotic dynamics such as those arising in cardiac arrhythmias. Additionally, the metabolic system is comprises a large-scale biochemical system which, when simplified to a few variables, also exhibits chaotic dynamics [17, 23]. For example, the metabolic pathway converts the free energy in glucose into adenosine triphosphate (ATP), which is then converted to adenosine diphosphate (ADP). For certain amplitudes and frequencies of sugar influx, the fluctuations in the concentration of ADP are chaotic [17]. Changes in the chaotic attractor's dimension may also indicate a pathology such as in epilepsy, where a "petit mal" seizure has been found to dramatically change the neural chaotic attractor and decrease its dimension [20, 21]. The analysis of chaotic dynamics present in chemical interactions, anatomical structure, and physiological systems allows for better physical understanding and modeling of systems for the characterization and control of diseases.

1.5 Chaos Maps

Various equations have been developed for the purpose of studying chaotic dynamics more in depth or mimicking those that occur in nature. In this chapter, traditional chaotic maps are defined. Sections 1 and 2 introduce the logistic and Hénon maps respectively, low-order discrete maps in 1 and 2 dimensions which have been widely used in chaos studies. Section 3 presents a more complex discrete map, the Ikeda map, which contains sinusoidal terms and describes instances of chaos in optics. Two continuous maps, the Lorenz map and the Mackey-Glass equation, are described in Sections 4 and 5. The multi-dimensional Lorenz differential equations are the basis of chaos theory and have led to the creation of various chaotic maps such as the Hénon map. The Mackey-Glass equation is used to represent chaotic series of high complexity, where the high order results from the delay in the differential equation.

1.4.1 Logistic Map

The logistic map, a simple non-linear system, depicts the population growth equation in discrete-time as:

$$x_{n+1} = rx_n(1-x_n), \tag{1.2}$$

where x_n characterizes the dimensionless population at time n. The equation is typically applied with $0 \le r \le 4$ such that x always maps to the interval [0,1]. At r=3 the logistic map is period-2 and period-doubling continues until r=3.569946 [12]. The chaotic regime begins at $x \approx 3.57$, but is interrupted by periodic windows, the intermittency route to chaos. This phenomenon can be observed in the bifurcation diagram in Figure 1.1.

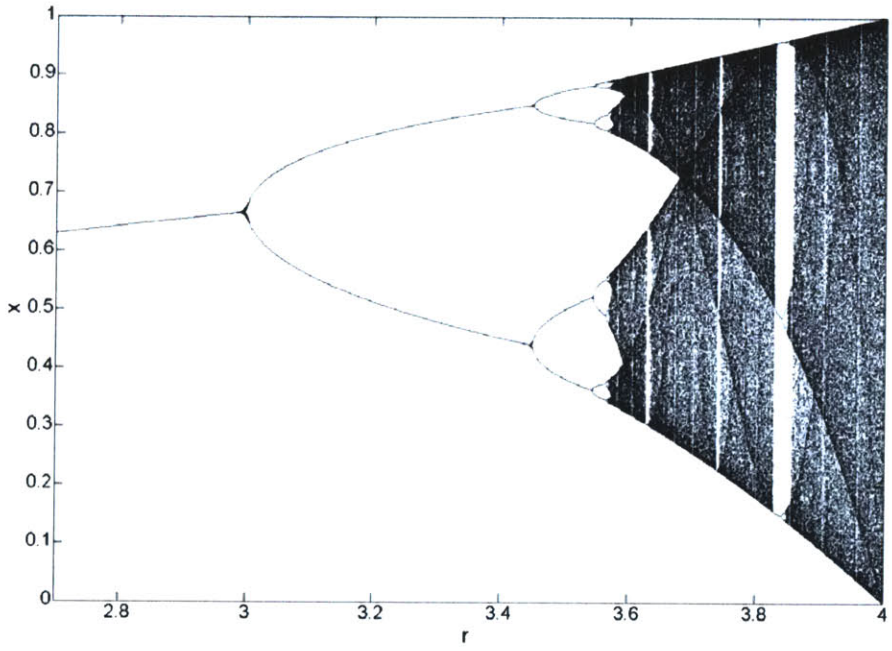

Figure 1.1. Bifurcation diagram for the logistic map.

1.4.2 Hénon Map

The Hénon map was developed as a manner of studying strange attractors, such as those described by Lorenz, in a two-dimensional discrete manner. The equations for this map are:

$$\begin{aligned} x_{n+1} &= y_n + 1 - ax_n^2 \\ y_{n+1} &= bx_n \end{aligned}, \tag{1.3}$$

where a is controlled to keep the system trajectories from escaping to infinity and b dictates the folding and contraction of the attractor [12]. Typically, b is kept constant at 0.3 while a is varied to characterize the system (a=1.4 is often used to describe a chaotic system). Contrary to the logistic map, the Hénon map is invertible, such that each point corresponds to a unique trajectory. The Hénon map is also dissipative and contains trajectories which diverge to infinity unlike the Lorenz map where all trajectories converge towards the attractor [24].

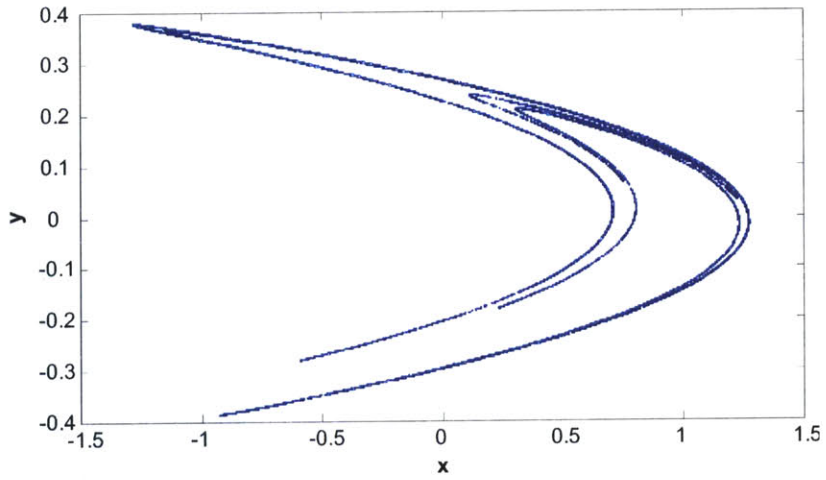

Figure 1.2. Chaotic attractor of the Hénon map for a = 1.4 and b = 0.3.

1.4.3 Ikeda Map

The Ikeda map demonstrates chaotic attractors in optics. Ikeda modified the traditional method of observing optical bistability, an example of first order phase transition in a system far from thermal equilibrium, and showed that the instabilities of light transmitted by a ring cavity systems exhibit chaotic behavior for certain parameters [25]. The Ikeda map is a two-dimensional map described by a complex number $z = x + iy$:

$$f(z) = p + B\exp\left(i\kappa - \frac{i\alpha}{1+|z|^2}\right)z. \tag{1.4}$$

The algorithm can also be written in two real dimensions [26]:

$$\begin{aligned} x_{n+1} &= p + B\left(x_n \cos t_n - y_n \sin t_n\right) \\ y_{n+1} &= B\left(x_n \sin t_n + y_n \cos t_n\right) \end{aligned}, \tag{1.5}$$

where the system is chaotic for certain values of B and t_n is described as:

$$t_n = \kappa - \frac{\alpha}{1 + x_n^2 + y_n^2}. \tag{1.6}$$

The values used were p = 1, κ = 0.4, and α = 6, while B was the variable parameter. The chaotic attractor of the Ikeda map is illustrated in Figure 1.3.

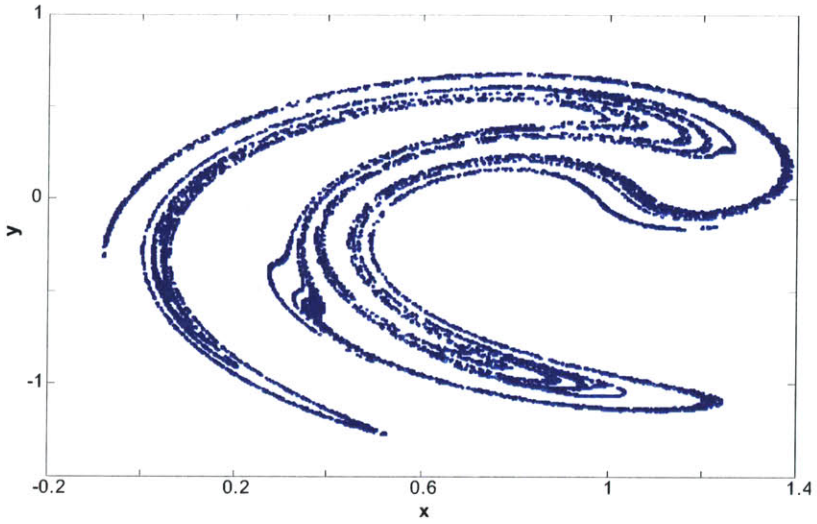

Figure 1.3. Chaotic attractor of the Ikeda map for B = 0.82.

1.4.4 Lorenz Map

The Lorenz equations are:

$$\begin{aligned} \dot{x} &= -\sigma x + \sigma y \\ \dot{y} &= -xz + rx - y \\ \dot{z} &= xy - bz \end{aligned}, \tag{1.7}$$

where σ (Prandtl number), r (Rayleigh number), and b greater than zero and the dot represents differentiation with respect to a dimensionless time.

In Lorenz's original study, he applied the model with the parameters σ = 10 and b = 8/3, in agreement with Saltzman's model [27]. These values were used by Lorenz, along with a time step of 0.01, for numerical integration in order to characterize the system's convective properties. Lorenz found certain parameters could yield solutions that oscillate irregularly, settling on a strange attractor with fractal dimension between 2 and 3. These oscillations occur for r values past the critical bifurcation:

$$r_H = \frac{\sigma(\sigma + b + 3)}{\sigma - b - 1}, \tag{1.8}$$

such that Lorenz published his results for the supercritical value r=28—$r_H \approx 24.74$ for the specific parameters used. There exist intermittent windows of periodicity for $28 < r < 313$. The three largest windows occur for r in the approximate intervals (99.524, 100.795), (145, 166), and (214.4, 313) [12].

The Lorenz equations resemble those from previous studies by Rayleigh and Saltzman which modeled flow in a layer of fluid of uniform depth with a constant temperature difference between the two surfaces. Each variable is proportional to a property of the system: x to the intensity of the convection motion, y to the temperature difference between currents, and z to the deviation from the linear temperature profile. A mechanical model of the Lorenz equations was developed in the 1970s [12]. The model consists of a waterwheel with leaking cups. Water is poured steadily into the cup at the top of the waterwheel and depending on the flow rate of the water the waterwheel can remain stationary, rotate steadily, or, for high flow rates, rotate erratically. Additional changes can be made to the model by modifying the brake on the wheel or changing the tilt of the table on which the waterwheel rests.

1.4.5 Mackey-Glass Equation

The Mackey-Glass equation describes physiological systems and characterizes acute diseases such as white-cell production dynamics and the irregular breathing pattern of Cheyne-Stokes respiration [28, 29]. The Mackey-Glass single-variable equation is [28]:

$$\frac{dx}{dt} = \frac{ax(t-\tau)}{1+x^n(t-\tau)} - bx(t), \tag{1.9}$$

where t is the time interval, τ is the delay dependence, and a, b, and n are parameters that can be altered to achieve periodicity or chaos. The complexity of the system relies heavily on the delay of the differential equation, which is proportional to the dimension of the chaotic attractor. The multistable property of the system causes a heavy reliance on the initial conditions, where periodicity or chaos can result from the same system with different initial conditions [30]. Similar to the Lorenz map, the integration step and sampling of the continuous-like signal affect the titration results. In this study, the Mackey-Glass signals were calculated as in a previous study with an integration step of 0.1 seconds, and sampling every 4 seconds [3]. A chaotic Mackey-Glass series is plotted in Figure 1.4.

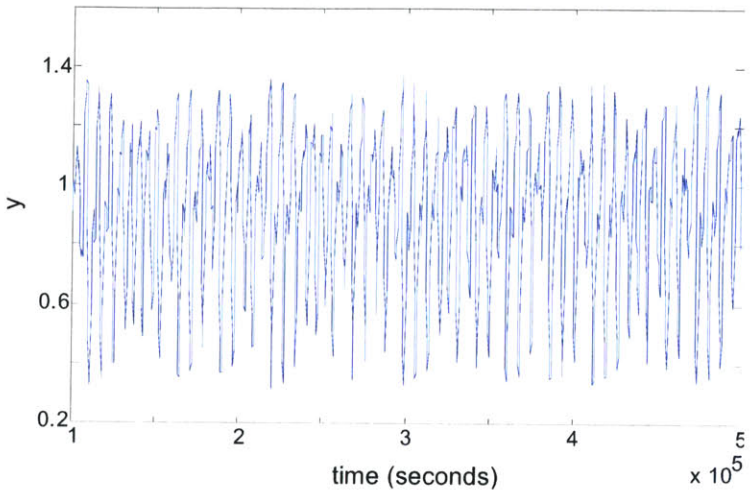

Figure 1.4. Mackey-Glass chaotic thousand-point series with a = 0.2, b = 0.1, n = 10.5.

Chapter 2 Nonlinearity and Chaos Detection Theory

The Volterra autoregressive series (VAR), a powerful tool for detecting nonlinearity comprises the basis of the algorithms for distinguishing dynamic and measurement noise in chaotic series. A summary of the theoretical basis of VAR, a modification on the traditional Volterra series proposed by Barahona and Poon, is presented in Section 1. The effect of noise on chaotic series cannot be studied without ensuring the contaminated signal is in fact chaotic. Section 2 describes the numerical titration technique [3], where the algorithm output provides sufficient proof of the existence of chaos in short, noisy series.

2.1 Volterra Autoregressive Series Theory

The Volterra autoregressive series (VAR) detects nonlinearity in short data series contaminated with additive and dynamic noise [31]. This method orthogonalizes the traditional Volterra series through a Gram-Schmidt procedure by applying the Wiener series expansion. The Volterra kernels can thus be estimated by recursively applying cross-correlation techniques, while introducing the limitation of a white noise Gaussian input of infinite length. The restriction on the input is eliminated by applying Korenberg's algorithm [32] which estimates the Volterra series for arbitrary signals. The VAR method moreover feeds the output as the delayed input into the Volterra series, allowing the current data point (x_n) be predicted by a polynomial expansion of previous points with degree d and memory κ:

$$\begin{aligned} x_n &= a_0 + a_1 x_{n-1} + a_2 x_{n-2} + \bullet\bullet\bullet + a_\kappa x_{n-\kappa} + a_{\kappa+1} x_{n-1}^2 + a_{\kappa+2} x_{n-1} x_{n-2} + \bullet\bullet\bullet + a_{M-1} x_{n-\kappa}^d \\ &\equiv \sum_{m=0}^{M-1} a_m z_m(n) \end{aligned}, \qquad (2.1)$$

where setting d =1 models a linear time series. The model can be modified to include additive dynamic (δ_n) and measurement (e_n) noise:

$$\tilde{x}_n = a_0 + a_1 \tilde{x}_{n-1} + a_2 \tilde{x}_{n-2} + \bullet\bullet\bullet + a_\kappa \tilde{x}_{n-\kappa} + a_{\kappa+1} \tilde{x}^2_{n-1} + a_{\kappa+2} \tilde{x}_{n-1} x_{n-2} + \bullet\bullet\bullet + a_{M-1} \tilde{x}^d_{n-\kappa} + \delta_n$$

$$\equiv \sum_{m=0}^{M-1} a_m \tilde{z}_m(n) + \delta_n \quad , \qquad (2.2)$$

and $y_n = \tilde{x}_n + e_n$

where $\tilde{x}_n$ is the orbit of the attractor including dynamic noise, and y_n is the observation after the inclusion of additive noise.

The goodness of fit of the models is quantified by the normalized sum-of-square errors:

$$\varepsilon(\kappa, d)^2 \equiv \sum_{n=1}^{N} (\hat{x}_n(\kappa, d) - y_n)^2 / \sum_{n=1}^{N} (y_n - \bar{y})^2 \quad . \qquad (2.3)$$

The optimal model is defined as that which minimizes the Akaike information criterion:

$$C(r) = \log \varepsilon(r) + r / N \quad . \qquad (2.4)$$

Two models are proposed to discriminate between stochastic chaos induced by dynamic noise and deterministic chaos in the presence of measurement noise respectively. Though the VAR algorithm cannot distinguish between dynamic and measurement noise, its equations seem to model dynamic noise better than measurement noise. One of the models implements the successive substitution VAR (SSVAR) algorithm, a modification on the VAR algorithm which is more responsive to measurement noise. The SSVAR algorithm iteratively applies the VAR algorithm to the synthesized data, subtracting an error term each time, until the VAR coefficients and the synthesized data converge. This ensures dynamic noise is not modeled in the synthesized data. Thus, for data contaminated with dynamic noise, as long as the error subtraction does not modify the underlying system dynamics, VAR should produce a lower error, and consequently a lower C(r), than SSVAR. For measurement noise, SSVAR should yield the lower C(r).

2.2 Detection of Chaos Level

Numerical titration [3] quantifies the intensity of chaos in a signal, in a manner similar to a chemical titration where the signal acts as the acid and noise acts as the base. This method presents several

advantages over traditional methods. Nonlinear measures such as detrended fluctuation analysis require long sets of data and complexity estimates such as entropy measures do not characterize the nonlinear properties of the signal. In addition, a positive Lyapunov exponent, the traditional measure for chaos detection and quantification, can only be accurately applied to ideal noise-free systems whereas numerical titration has proven an effective measure of chaos for noisy, short data sets.

Noise limit (NL), the output of numerical titration, is a relative measure of the chaos intensity in the series, where a positive NL is sufficient to confirm the existence of chaos. The input to numerical titration is a time series, such as heart rate variability for disease screening. Nonlinear detection is performed on the input with the Volterra autoregressive series, where the input is considered nonlinear if the approximated nonlinear model yields a better fit than the linear model. The best fitting signal is determined by the Akaike information criterion and significance is established with an F-test. If the signal is determined to be linear, it is non-chaotic and NL=0. For a nonlinear signal, a small amount of noise — 1% of the variance— is added to the signal and the nonlinear detection is performed again. The noise addition and nonlinear detection are recursively performed until the signal is not determined to be nonlinear. The positive NL thus characterizes the amount of noise necessary to mask the signal's chaotic dynamics. The numerical titration process is illustrated in Figure 2.1.

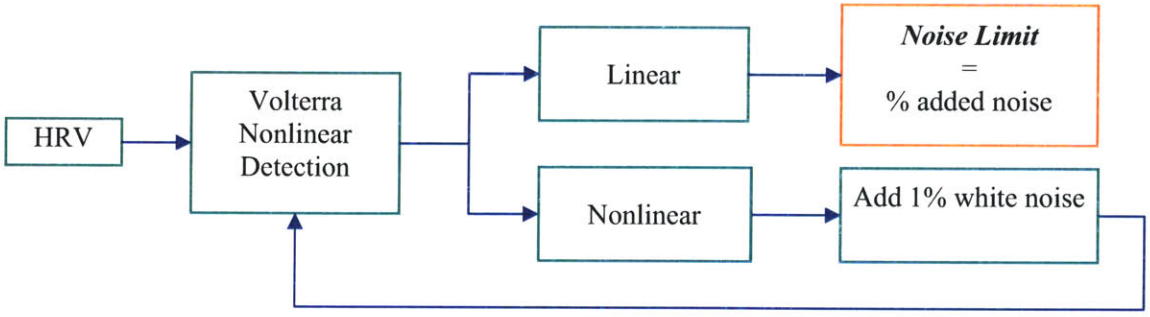

Figure 2.1. Numerical titration algorithm

The numerical titration technique has been proven successful in yielding NL>0 for signals with a positive Lyapunov exponent in standard routes to chaos for several maps including the logistic map, Curry-Yorke discrete map, Mackey-Glass equations, and Lorenz map. In addition, numerical titration has successfully

identified chaos in high order systems such as a Mackey-Glass map with dimension twenty [3]. However, it should be noted that titration cannot provide insight into the dynamics of a system with a negative Lyapunov exponent, where nonlinearity is not detected.

Chapter 3 Numerical Simulation Results for Characterization of the Chaotic Maps

This chapter explains the parameter selection procedure for the discrimination algorithm, the sampling of the Lorenz map for the creation of a chaotic series, and the chaotic maps. Section 1 examines the effect of the integrator and sampling step for continuous maps, specifically the Lorenz map, on the detected chaos level. The maps for testing the noise discrimination algorithms were chosen such as to represent various non-chaotic and chaotic regions as well as all of the main routes to chaos. The choice of parameters for the discrete and continuous maps is explained in Section 2. Finally, Section 3 investigates the effect of dynamic and measurement noise on periodic and chaotic regions of the logistic and Hénon maps.

3.1 Effect of integrator, integration step, and discretization on the Lorenz map

The nonlinearity detection step in numerical titration requires a discrete signal with uniform spacing in time. For continuous maps this implies a downsampling step, where the discrete signal to be titrated contains uniformly-spaced samples of the continuous-like integrated signal. Thus the integrator, integration step, and discretization affect the resulting map and its level of chaos. The choice of integrators is limited by the necessity of a fixed-time solver. The choice of integrator—Euler's method (first order), Heun's method (second order), or fifth order Runge-Kutta—affects the proximity of the discrete-time integration to a continuous-time integration. The higher order incorporates more terms into the integration and thus provides the most accurate computations. The choice of integration step is essential due to similar reasons: a smaller integration step will yield a better approximation of the discrete signal to a continuous signal, yet a decrease in the integration step causes a significant increase in computation time. The discretization, the sampling of the signal after integration, has a different effect on the system since undersampling prevents an accurate description of system dynamics and oversampling may cause numerical titration to falsely identify the system as non-chaotic since the Volterra series would be calculated based on linearized segments.

Figure 3.1 illustrates the importance of the integrator order and integration step in the Lorenz map. Letellier found that though any sampling of less than 0.040 seconds will fulfill the Nyquist criterion, the upper value of the discretization step for a first-order integrator (0.0265 seconds) is less than the ideal value for a second-order integrator (0.064 seconds), such that higher-order integrators can be applied with larger discretization steps while preserving the chaotic dynamics of the Lorenz map [33]. The first-order integrator, the Euler method, does not recognize the chaotic signals for the larger integration step and identifies non-chaotic regions as chaotic for the smaller integration step. The importance of the integration step is seen most clearly for the second-order integrator, where the smaller integration step classifies all the regions except for one (r = 146) as chaotic or non-chaotic. The high accuracy achieved with the fifth-order integrator diminishes the role of the integration step such that both integration steps only misclassify one non-chaotic signal as chaotic with a miniscule noise limit (NL<2).

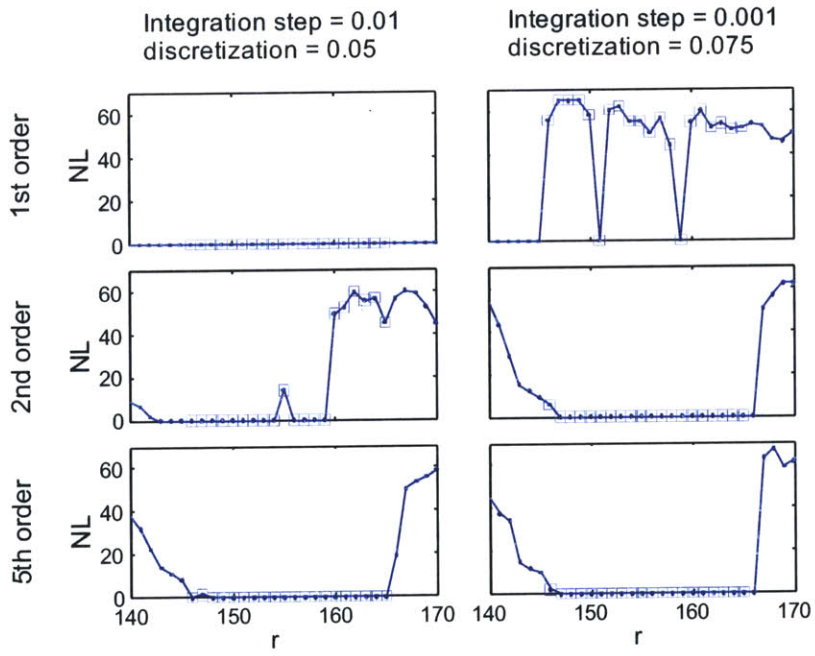

Figure 3.1. The results of different integration of the Lorenz map are classified by order of integrator (rows) and integration step (columns). The squares represent points that are not chaotic (NL should be zero).

3.2 Choice of Parameters for Chaotic Maps

The parameters for the different maps were chosen such as to describe various non-chaotic and chaotic regions. The variable parameter for the logistic map, r in

$$x_{n+1} = rx_n(1-x_n), \tag{3.1}$$

was chosen to convey four different regions of the bifurcation diagram. The chosen parameter values and the map region for the well-studied logistic map were: r=3.2 (period-2), r=3.5 (period-4), r=3.568759 (period-16), r=3.7 (low chaos), r=3.8282 (intermittency), r=3.9 (high chaos) [12]. The parameters for the other maps were chosen by examination of the chaos level at different values. Graphs of the noise limit for different parameter values of each map are plotted in Figure 3.2 where the red circles indicate the parameters used in the study.

The variable parameter in the Hénon map, a in

$$\begin{aligned} x_{n+1} &= y_n + 1 - ax_n^2 \\ y_{n+1} &= bx_n \end{aligned}, \tag{3.2}$$

was chosen as to represent a periodic region (a=1), a low chaos region (a=1.08), a non-chaotic region surrounded by chaos (a=1.25), and a highly chaotic region (a=1.4).

The variable parameter for the Ikeda map, B in

$$\begin{aligned} x_{n+1} &= p + B\left(x_n \cos t_n - y_n \sin t_n\right) \\ y_{n+1} &= B\left(x_n \sin t_n + y_n \cos t_n\right) \end{aligned}, \tag{3.3}$$

was chosen as to represent a series long before chaos is reached (B=0.5), a periodic series close to the start of chaotic dynamics (B=0.62), a highly chaotic series (B=1.25), and a non-chaotic series surrounded by chaos (B=1.4).

The variable parameters for the continuous series, the Lorenz map and the Mackey-Glass equation were similarly chosen to encompass non-chaotic regions away from chaos, various chaos levels, and low or no chaos regions where a slight parameter change in either direction would largely increase the chaos level. In the Lorenz map

$$\begin{aligned} \dot{x} &= -\sigma x + \sigma y \\ \dot{y} &= -xz + rx - y, \\ \dot{z} &= xy - bz \end{aligned} \tag{3.4}$$

r was chosen as 14, 28, 150 and 170. The Mackey-Glass equation

$$\frac{dx}{dt} = \frac{ax(t-\tau)}{1+x^n(t-\tau)} - bx(t) \tag{3.5}$$

was analyzed for n=8, 9, 9.75, and 10.5. The fewer points in the Mackey-Glass map in Figure 3.2 results from the extensive computations required to create the series.

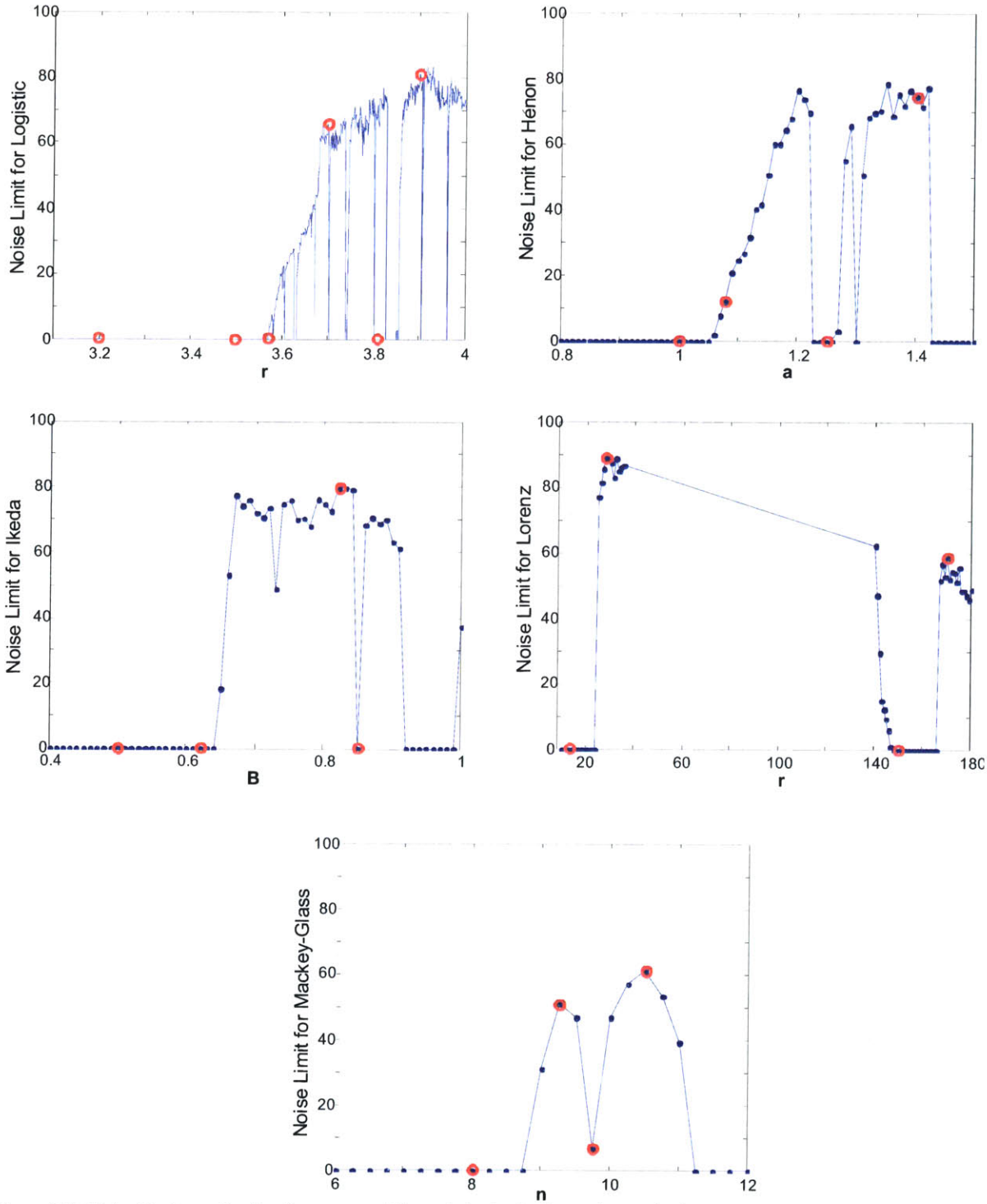

Figure 3.2. Noise limit graphs for chaos maps. The red circles indicate the particular parameters that were analyzed.

3.3 Effect of Dynamic and Measurement Noise on the Logistic and Hénon Maps

A positive noise limit can be a result of an intrinsically chaotic system or a system driven into chaos by noise. Similarly, a non-chaotic system can be such because of the linearity of the signal or randomness induced by measurement noise. Though the noise-free system can never be perfectly extracted from a noisy signal, the identification of the driving noise in the system—measurement or dynamic—can provide insight into system properties. The following sections describe the effects of measurement and dynamic noise on the logistic map and the Hénon map, examining different routes to chaos and signals with diverse chaos intensities.

3.3.1 Definition of Dynamic and Measurement Noise

Dynamic noise was defined as noise added in every time step such that it affected the calculation of future data points. For multidimensional maps such as the Hénon map, noise was only added in one of the dimensions:

$$\begin{aligned} x_{n+1} &= y_n + 1 - ax_n^2 + \delta_{n+1} \\ y_{n+1} &= bx_n \\ \hat{x} &= x \end{aligned}, \tag{3.6}$$

where δ is the dynamic noise component and $\hat{x}$ is the observation. Measurement noise was added to a complete noise-free map, such that the noise was superimposed on the signal to form the observation and did not affect the signal dynamics. The logistic map contaminated with measurement noise can be represented as:

$$\begin{aligned} x_{n+1} &= rx_n(1 - x_n) \\ \hat{x} &= x + \varepsilon \end{aligned}, \tag{3.7}$$

where ε is the measurement noise component and $\hat{x}$ is the observed series. The applied noise was random Gaussian noise generated in Matlab.

3.3.2 Effect of Noise on the Logistic Map

The intensity of chaos in a signal is dependent both on the chaotic background, the intensity of the noise, and the type of noise contaminating the system. The following figures illustrate this dependence with the logistic map. When measurement noise is added to a non-chaotic signal such as the logistic map in the period-doubling regions (Figure 3.3) the map dynamics are not changed, and the added randomness of the noise is not mistaken as nonlinearity such that the noise limit remains at zero. However, measurement noise plays an important role in the chaos intensity of the maps in the chaotic regimes. As can be seen in Figure 3.3, as the noise variance increases, the chaos level, measured by the noise limit, decreases. The noise limit will be zero when the randomness of the noise overshadows the chaotic dynamics of the signal. Thus, the intensity of the underlying chaotic dynamics is proportional to the noise variance required to drive the chaos level to zero. This relation is illustrated in Figure 3.3, where the seemingly linear trend of decreasing noise limit with increasing noise variance intercepts the x-axis at the highest noise variance for the most chaotic map (r=3.9).

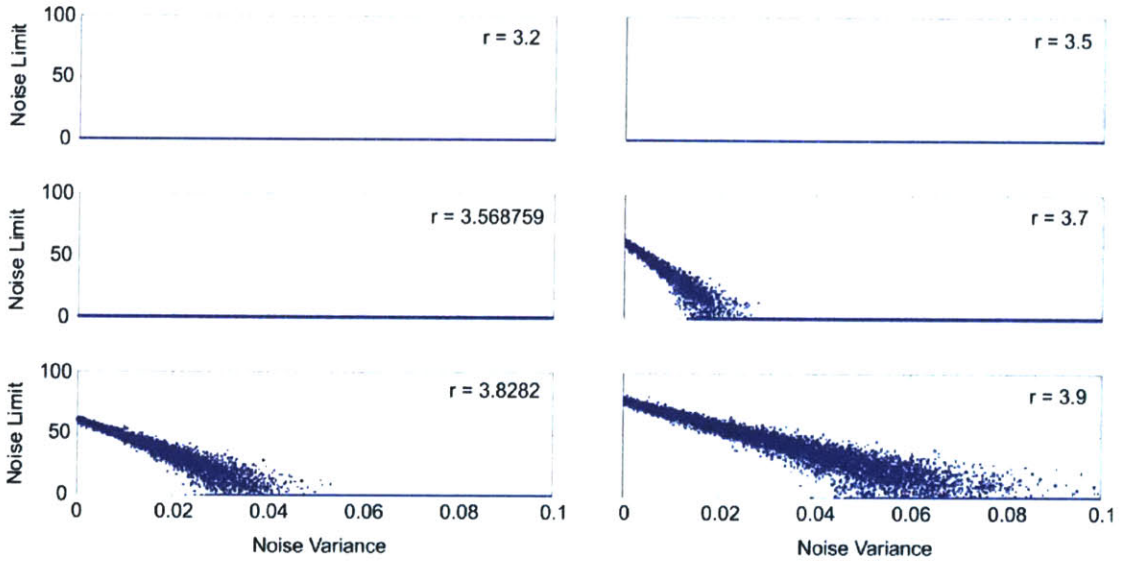

Figure 3.3. Effect of increasing measurement noise on the detected intensity of chaos for different regions of the logistic map.

Contrary to measurement noise, which affects the noise limit of already chaotic maps, the addition of dynamic noise has the largest effect on non-chaotic maps. Figure 3.4 shows slight or no increase in the noise limit of maps that are intrinsically chaotic after the addition of dynamic noise. However, noise-free

non-chaotic maps become increasingly chaotic with the inclusion of dynamic noise, saturating at a maximum noise limit value for high noise variances. This effect can be seen in Figure 3.4, where the noise limit increases more rapidly with increasing noise for maps which are closer to chaotic regions, where the noise limit for the period-16 logistic map (r=3.568759) saturates for lower noise variances than the noise limit for the period-2 logistic map (r=3.2).

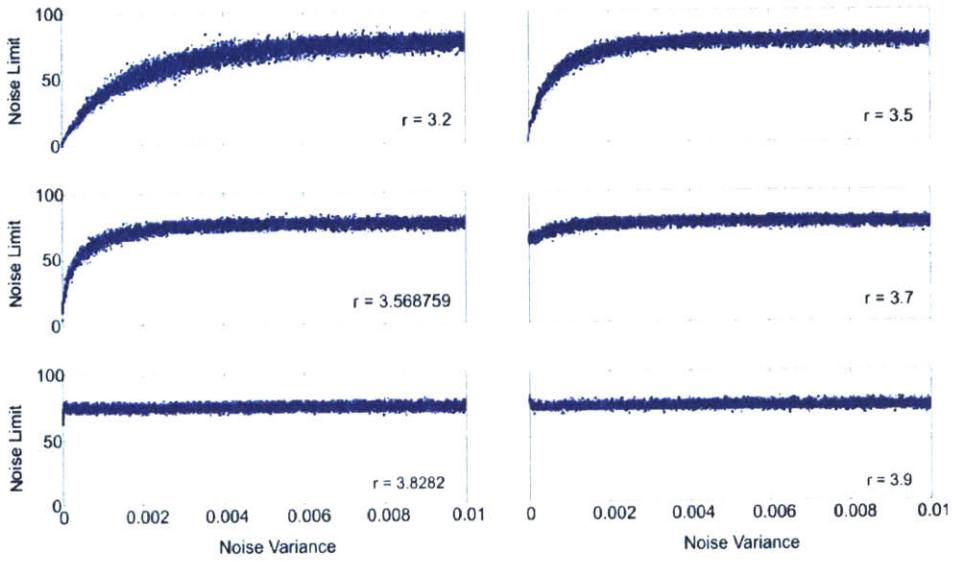

Figure 3.4. Effect of increasing dynamic noise on the detected intensity of chaos for different regions of the logistic map.

3.3.3 Effect of Noise on the Hénon Map

The effect of measurement noise on the detected chaos level of the Hénon map is similar to that of the logistic map. Periodic regimes retain a noise limit of zero while chaotic maps experience a decrease in the noise limit with an increase in the measurement noise variance. However, as can be seen in Figure 3.5 the chaotic region with the highest noise limit (a=1.4) never becomes non-chaotic in the experimental noise variance range. This suggests a chaotic system more robust to measurement noise than the logistic map with similar noise-free noise limits.

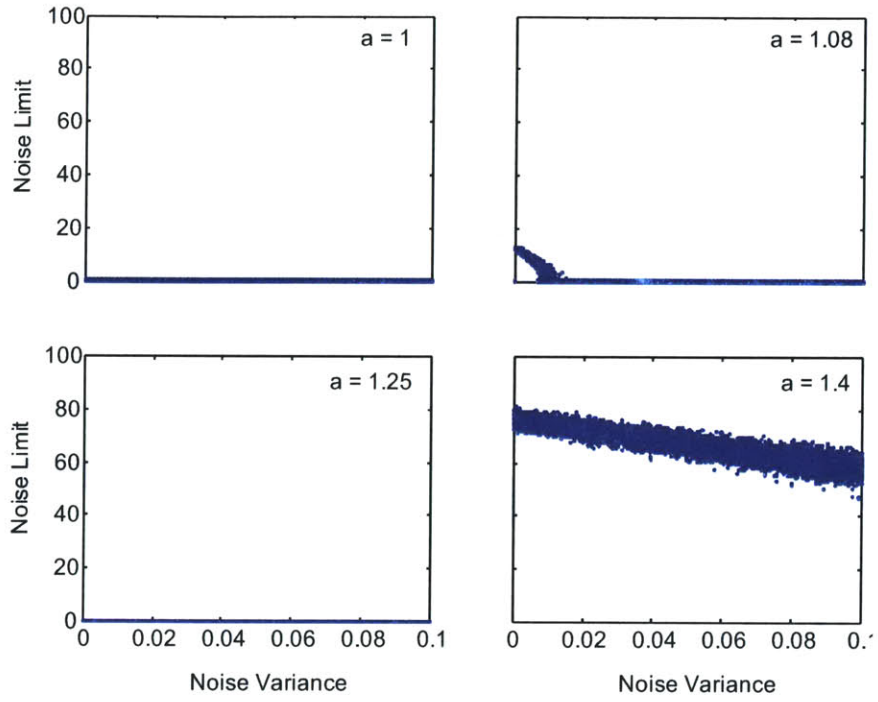

Figure 3.5. Effect of increasing measurement noise on the detected intensity of chaos for different regions of the Hénon map with b=0.3.

As with the logistic map, the addition of dynamic noise to the Hénon map results in increasing noise limit for non-chaotic series, as can be seen in Figure 3.6. In the period-doubling route to chaos (a=1) and the region with low noise-free noise limit (a=1.08) the noise limit increases slowly with increasing noise variance, yet the noise limit never saturates as it does with the logistic map in the experimental noise variance region. The lesser effect of dynamic noise on the Hénon map than the logistic map could be due to the 2-dimensionality property of the Hénon map, since noise is only added to the x-dimension. The bottom panels in Figure 3.6 do however illustrate a saturated noise limit for higher noise variances. The saturation point is the noise limit when a=1.4, representing the highest level of chaos that can be achieved in the Hénon map. The two points with noise limit less than 20 in the Hénon map with a=1.4 in Figure 3.6 result from divergence of the Hénon map, where the map can no longer be accurately represented by a polynomial and only a small amount of noise is needed to overshadow the nonlinear dynamics. However, these points can be disregarded since the other 9998 series yielded similar noise limits and the study focuses on signals that do not diverge such as physiological signals. The fast saturation for the periodic region of a=1.25 results from the proximity to regions with a high noise limit, where a small amount of noise drives the system out of periodicity and into the highly chaotic attractor.

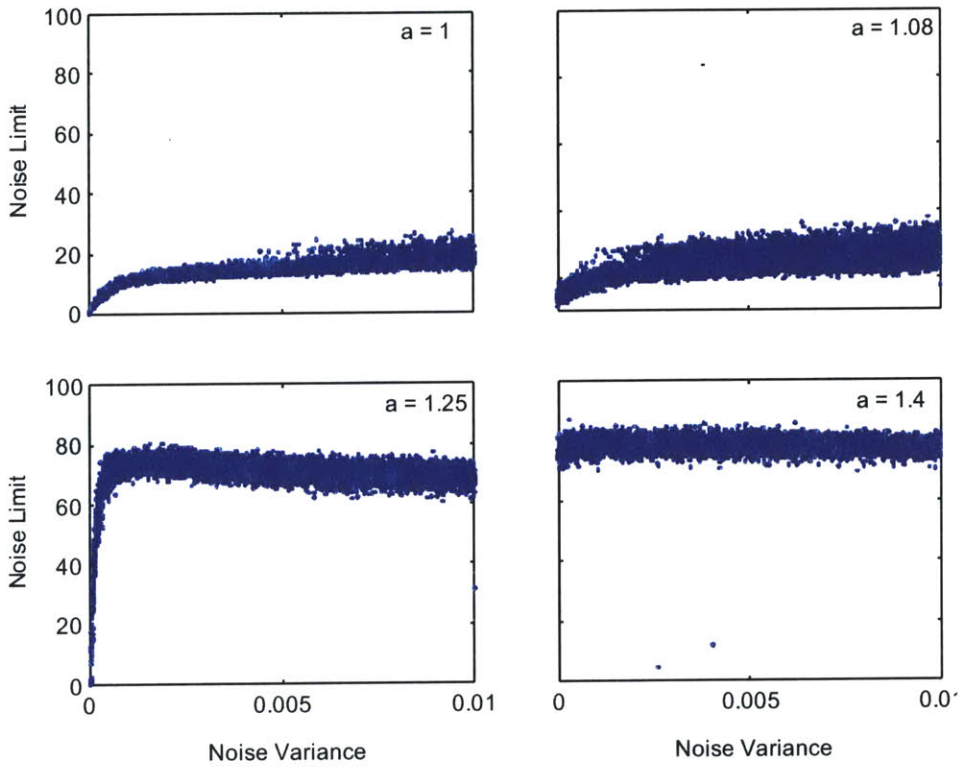

Figure 3.6. Effect of increasing dynamic noise on the detected intensity of chaos for different regions of the Hénon map with b=0.3.

Chapter 4 Noise Discrimination Algorithms

The Volterra autoregressive series described in Chapter 2 includes an error term to account for dynamic noise in the system, such that a new method, the successive substitution Volterra autoregressive series (SSVAR) algorithm is proposed as a method that eliminates the dynamic noise term in the polynomial approximation by a series of iterations. Sections 1 and 2 focus on the algorithms implemented for modeling of series with dynamic and measurement noise. Section 3 introduces some of the challenges that occur from modeling a series with the successive substitution VAR algorithm, and the best discrimination algorithms, for which the results are presented in the next chapter, are described. The best noise identification algorithm determines whether a signal is mainly contaminated with dynamic or measurement noise by the progression of the cost function curves in the different iterations instead of the best fitting model.

4.1 Volterra Autoregressive Series for Detection of Dynamic Noise

The Volterra autoregressive series (VAR) algorithm aids in the detection of stochastic chaos by including a parameter for dynamic noise in the polynomial expansion. The underlying dynamics of a physiological system such as the heart rate can be contaminated by additive dynamic noise (δ_n) due to various physiological processes. Since the noise affects the physiological output at each time step, it is accounted for in the recursive calculation of each time index.

$$\begin{aligned} \tilde{y}_n &= a_0 + a_1 \tilde{y}_{n-1} + a_2 \tilde{y}_{n-2} + \bullet\bullet\bullet + a_K \tilde{y}_{n-K} + a_{K+1} \tilde{y}^2_{n-1} + a_{K+2} \tilde{y}_{n-1} y_{n-2} + \bullet\bullet\bullet + a_{M-1} \tilde{y}^d_{n-K} + \delta_n \\ &\equiv \sum_{m=0}^{M-1} a_m \tilde{z}_m(n) + \delta_n \end{aligned} \tag{4.1}$$

The VAR algorithm was implemented as:

Input: observed time series y_n

1. Derive z_m from y_n.
2. Using the Korenberg algorithm, calculate the Volterra coefficients a_m.
3. Synthesize the time series $\tilde{y}_n$.

4. Based on y_n and $\tilde{y}_n$, measure the goodness-of-fit with $C(r)$.

Output: synthesized time series $\tilde{y}_n$, $C(r)$

4.2 Successive Substitution Volterra Autoregressive Series for Detection of Measurement Noise

The successive substitution Volterra autoregressive series (SSVAR) algorithm assumes a series free of stochastic dynamic noise, but includes an additional parameter for measurement noise. Measurement noise in a physiological recording is due specifically to the recording device and is thus modeled as deterministic noise.

$$x_n = a_0 + a_1 x_{n-1} + a_2 x_{n-2} + \bullet\bullet\bullet + a_K x_{n-K} + a_{K+1} x_{n-1}^2 + a_{K+2} x_{n-1} x_{n-2} + \bullet\bullet\bullet + a_{M-1} x_{n-K}^d$$
$$\equiv \sum_{m=0}^{M-1} a_m z_m(n) \qquad (4.2)$$

and $y_n = x_n + e_n$

The SSVAR algorithm was implemented as:

Input: observed time series y_n

1. Set $\hat{x}_n = y_n$.
2. Use VAR to find $\hat{a}_m$ and synthesize $\hat{y}_n$.
3. Set $\hat{x}_n = \hat{y}_n$.
4. Repeat 2-3 until $\hat{a}_m$ and $\hat{y}_n$ converge.
5. Based on y_n and $\hat{y}_n$, measure the goodness-of-fit with $C(r)$.

Output: synthesized time series $\hat{y}_n$, $C(r)$

A percentage of the error, 1 – modeling error correction factor (MEC), was subtracted from the synthesized data series at each iteration. This correction is necessary to prevent the elimination of underlying dynamics of the system while reducing the numerical error in the computations. Convergence between the VAR coefficients and the synthesized data series was defined as the two vectors having a

difference of less than a given threshold. The effects of the MEC and threshold on the output are further explained in Section 4.1.

4.3 Effect Successive Substitution Volterra Autoregressive Series Parameters and Noise Discrimination Algorithm

The threshold and modeling error correction factor (MEC) play an important role in the convergence and effectiveness of SSVAR. The threshold represents the maximum percentage difference between consecutive iterations of SSVAR to define convergence. An increase of the threshold value from 10% to 15% and the MEC from 50% to 80% individually decreased the error in SSVAR, yielding a C® similar to that of VAR for a higher noise variance. The increase in threshold allowed for SSVAR convergence after fewer iterations, and thus a better data approximation (previous results showed excessive iterations to have a degenerative effect on the data modeling). The increase in MEC recognized most of the error is attributed to modeling and what would be physiologic factors such as polynomial approximation and a dynamic noise component respectively. The loss of the physiologic component was minimized by reducing the percentage of error attributed to the additive noise without significantly increasing the number of necessary iterations for convergence.

The nonlinear models produced by SSVAR rarely better fit the data than those resulting from the VAR algorithm. The addition of dynamic noise has a larger impact on the signal dynamics than the addition of measurement noise, such that the noise variance threshold for which both algorithms result in comparable performance is much higher for additive noise than dynamic noise. Modeling of the signal with the SSVAR algorithm presents an additional challenge in the determination of the ideal number of iterations before convergence. Excess iterations lead to the accumulation of modeling and numerical errors, where the modeling of complicated dynamics will progressively worsen causing the signal approximation to collapse to zero. This phenomenon exists for both measurement and dynamic noise with large variances. Figure 4.1 illustrates one such example of 100 points of a logistic map with dynamic noise (variance = 0.008) along with the estimated signal by SSVAR after 31 iterations.

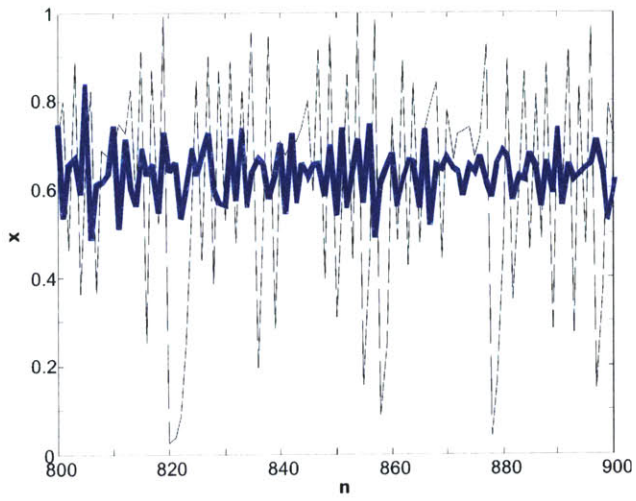

Figure 4.1. Logistic map with dynamic noise (thin, black line) and SSVAR estimation (thick, blue line) after 31 iterations.

An alternate detection scheme based on the identification of stochastic versus measurement noise was developed to avoid underfitting the data due to increasing computational errors. A signal is identified as dominated by measurement noise when the fit of the signal estimated by SSVAR improves at any time before convergence. The improvement of fit is measured by identifying a decrease of the SSVAR *C*® minimum in any of the iterations. Just as a better fit with the SSVAR algorithm than the VAR algorithm requires iterations such that both models produce different approximations, the new noise identification algorithm requires the SSVAR algorithm to iterate in order to identify any decrease in the *C*® minimum. In addition, the noise must not be so large that the signal is no longer nonlinear since a linear model would fit the data better than VAR or SSVAR.

The determination of the detection scheme is better explained through further examination of the cost function curves for the different iterations of SSVAR. The following figures illustrate the *C*® curves for the logistic map with dynamic or measurement noise. In the case where dynamic noise is added to the logistic map, iterations of the SSVAR algorithm cannot yie;d a better fit than the VAR algorithm. Instead, consecutive iterations of SSVAR increase the modeling error, monotonically worsening the fit of the signal. The cost functions for the first 8 iterations of SSVAR for a logistic map with dynamic noise are illustrated in Figure4.2.

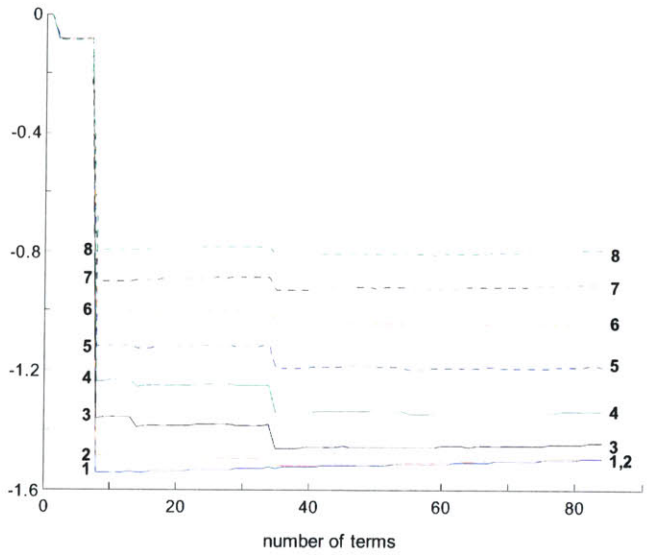

Figure 4.2. Cost functions of SSVAR. The signal is a logistic map with dynamic noise (variance = 0.003). The numbers to the left and right of each cost function represent the index of the first eight iterations.

Though modeling error also plays a role in signals with measurement noise, the SSVAR algorithm initially improves the fit of the data as predicted by the theoretical basis of the algorithm. However, the number of times the fit is improved and the iteration in which the improvement begins varies with the signal and added noise. In the same manner, convergence of the SSVAR algorithm after the improvement in fit of the approximation to the observed data series is limited to certain series contaminated with noise of low variance, where the noise variance at which the iterations become detrimental depends on the specific map and the level of chaos. The SSVAR cost functions for a logistic map with measurement noise (variance = 0.03) which converged after eight iterations are plotted in Figure 4.3. The first iteration, the same model as determined by VAR, is plotted as the thick, blue line.

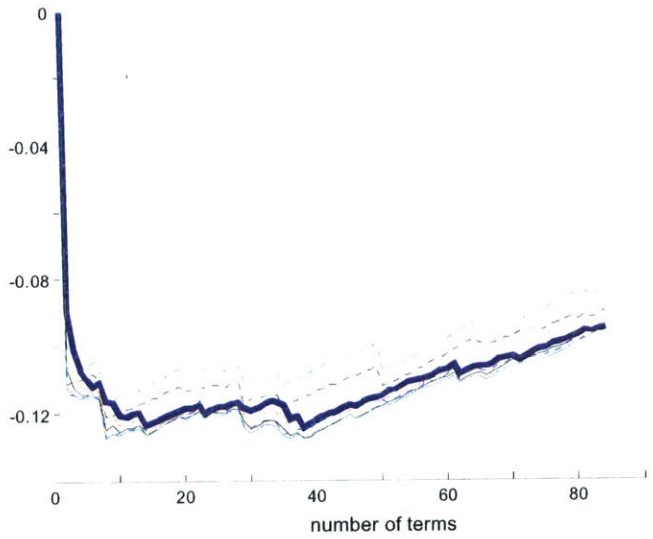

Figure 4.3. Cost functions of SSVAR for measurement noise. The signal is a logistic map with measurement noise (variance = 0.03). The thick blue curve is the cost function of the first iteration.

A segment of Figure 4.3 is enlarged in Figure 4.4. This segment plots the minimum of $C®$ for many of the iterations along with the iteration number. The minimum (best fitting model) occurs in the third iteration, after which the modeling error prohibits further improvement of the fit.

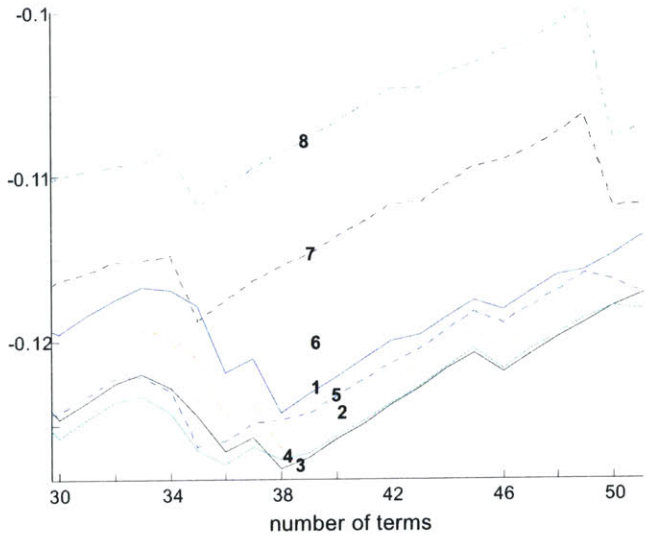

Figure 4.4. Close-up of SSVAR cost functions for measurement noise. The signal is a logistic map with measurement noise of variance 0.03. The iteration numbers of SSVAR are written in the middle of the curves.

The cost functions of SSVAR for dynamic and measurement noise can also be characterized by their different shapes. The difference arises from the form of the Volterra autoregressive series, where the polynomial series does not accurately represent measurement noise such that the noise will be incorrectly included in the calculation of the polynomial terms. This explains the sloping of the SSVAR $C_{\mathbb{R}}$, where the fit momentarily improves with increasing number of terms but rapidly deteriorates for the overfitted polynomials with excess number of terms.

Chapter 5 Results and Discussion of Noise Discrimination Algorithms

Discrimination between deterministic and stochastic noise was determined by the evolution of the cost function with consecutive iterations of the SSVAR algorithm, where deterministic noise was identified by a decreasing cost function at any iteration. The noise discrimination algorithm was tested on all of the non-chaotic and chaotic series defined in Section 4.3. This chapter presents the results and limitations for the algorithms as well as several suggestions of future work which could increase the accuracy of noise discrimination algorithms. Section 1 defines the algorithm parameters and noise levels used in the analysis. The individual results for measurement and dynamic noise are also presented in Section 1, whereas Section 2 delves into the limitations of the algorithms and how these limitations affected the analysis for the various chaotic maps. Section 3 sets the base for future work in discrimination of measurement and dynamic noise. Several improvements on the current algorithm are presented as well as suggestions of other algorithms which might prove to be more effective in identifying the noise characteristics in the chaotic signal.

5.1 Results of Noise Identification Algorithm on Chaotic Maps

SSVAR was executed with a modeling error correction factor (MEC) of 0.8 and a threshold of 10%. The conservative MEC preserved the underlying dynamics and the low threshold increased the number of iterations prior to convergence. Initial analysis yielded the fit of the data for SSVAR exclusively worsened for excessive iterations such that the number of iterations was limited to 20. In order to reduce the necessary number of computations, numerical titration was performed with degree 2 and memory 5 for the logistic and Hénon maps, both of which are of the Volterra form. The numerical titration for the Ikeda, Lorenz, and Mackey-Glass maps was performed with degree 3 and memory 6 as in [3], where the longer polynomial form was necessary to detect the nonlinear dynamics. All the analyzed series contained 1000 points. The number of series that were analyzed depended on the required computations for each map, such that the step in noise variance was increased in the more computation intensive maps. The range and step of the noise variance for each map are listed in Table 5.1.

TABLE 5.1. MEASUREMENT AND DYNAMIC NOISE VARIANCES TESTED FOR THE CHAOTIC MAPS.

Map	Dynamic Noise	Measurement Noise	Noise Variance range	Noise Variance step	Number of series
Logistic	X		[1e-6 1e-2]	1e-6	10000
Logistic		X	[0 1e-1]	1e-5	10001
Hénon	X		[1e-6 1e-2]	1e-6	10000
Hénon		X	[0 1e-1]	1e-5	10001
Ikeda	X		[1e-6 1e-2]	5e-6	2000
Ikeda		X	[0 1e-1]	5e-5	2001
Lorenz	X		[1e-6 1e-2]	1e-4	100
Lorenz		X	[0 1e-1]	1e-3	101
Mackey-Glass	X		[1e-5 1e-2]	1e-5	1000
Mackey-Glass		X	[0 1e-1]	1e-4	1001

The results of SSVAR analysis for dynamic noise are shown in Table 5.2 for the various chaotic maps. The table shows the number of tested maps that had a positive noise limit (chaotic), the number of maps where the SSVAR analysis yielded convergence in 1 iteration (SSVAR produced the same result as VAR), and the number of maps where the cost function for SSVAR decreased at any iteration.

TABLE 5.2. SSVAR RESULTS FOR DYNAMIC NOISE.

Map	Parameter	Noise-free NL	No. of series with NL>0	No. of series converging in 1 iteration	No. of series with decreasing C(r)
Logistic	r = 3.2	0	9999	2583	15
Logistic	r = 3.5	0	9999	1268	4
Logistic	r = 3.568759	0	9999	1021	2
Logistic	r = 3.7	60.2	10000	599	0
Logistic	r = 3.8282	61.6	10000	234	1
Logistic	r = 3.9	78.2	10000	89	0
Hénon	a = 1	0	9990	84	73
Hénon	a = 1.08	12.2	10000	2	1
Hénon	a = 1.25	0	9996	3	0
Hénon	a = 1.4	74.8	7737	6	0
Ikeda	B = 0.5	0	1999	1010	827
Ikeda	B = 0.62	0	1999	680	1178
Ikeda	B = 0.82	78.8	1998	0	1562
Ikeda	B = 0.85	0	1921	8	831
Lorenz	r = 14	0	26	25	0
Lorenz	r = 28	92.4	100	0	1
Lorenz	r = 150	0	100	0	48
Lorenz	r = 170	60.4	100	0	43
Mackey-Glass	n = 8	0	998	998	-

Mackey-Glass	n = 9	28.4	998	998	-
Mackey-Glass	n = 9.75	7.8	1000	1000	-
Mackey-Glass	n = 10.5	56.4	1000	1000	-

The results of SSVAR analysis for measurement noise are shown in Table 5.3 for the various chaotic maps.

TABLE 5.3. SSVAR RESULTS FOR MEASUREMENT NOISE.

Map	Parameter	Noise-free NL	No. of series with NL>0	No. of series converging in 1 iteration	No. of series with decreasing C(r)
Logistic	r = 3.2	0	0	-	-
Logistic	r = 3.5	0	0	-	-
Logistic	r = 3.568759	0	0	-	-
Logistic	r = 3.7	60.2	1824	25	1799
Logistic	r = 3.8282	61.6	3469	7	3458
Logistic	r = 3.9	78.2	6348	3	5987
Hénon	a = 1	0	0	-	-
Hénon	a = 1.08	12.2	970	1	969
Hénon	a = 1.25	0	0	-	-
Hénon	a = 1.4	74.8	10001	1	10000
Ikeda	B = 0.5	0	0	-	-
Ikeda	B = 0.62	0	0	-	-
Ikeda	B = 0.82	78.8	1976	0	1776
Ikeda	B = 0.85	0	650	1	564
Lorenz	r = 14	0	0	-	-
Lorenz	r = 28	92.4	101	0	0
Lorenz	r = 150	0	0	-	-
Lorenz	r = 170	60.4	101	0	101
Mackey-Glass	n = 8	0	0	-	-
Mackey-Glass	n = 9	28.4	625	325	300
Mackey-Glass	n = 9.75	7.8	41	41	-
Mackey-Glass	n = 10.5	56.4	2859	234	2625

The accuracy of detection for each parameter set of the chaotic maps can be seen in Figure 5.1. The dark bars indicate presence of dynamic noise while light bars with dark outline indicate presence of measurement noise. The asterisks in the figure do not represent 0% accuracy, but rather tests that could not run due to all non-chaotic series or all convergence in one iteration in the presence of dynamic (blue asterisk) or measurement (red asterisk) noise.

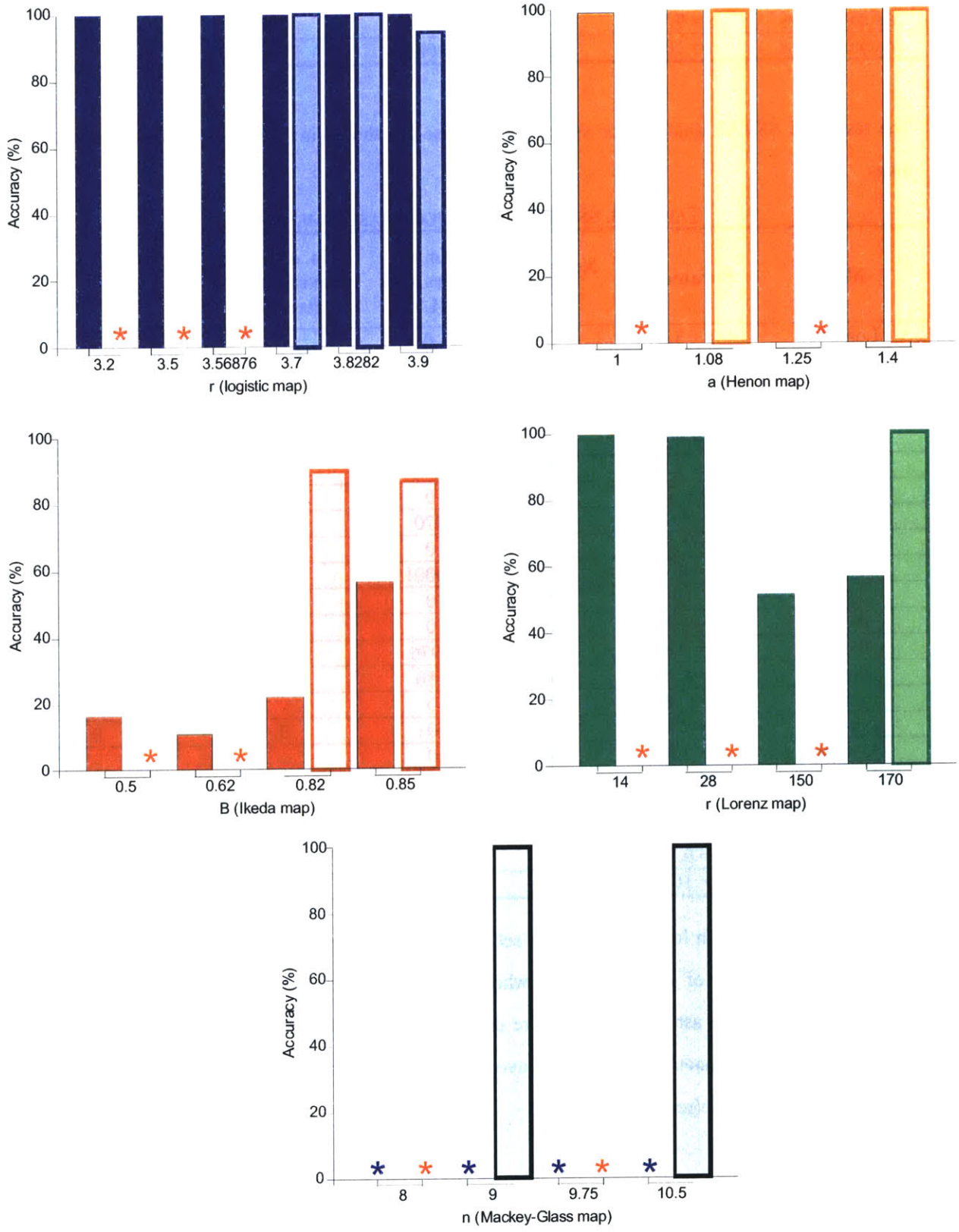

Figure 5.1. Accuracy of noise identification for chaos maps with dynamic and measurement noise.

The overall accuracy of the algorithm for the different maps in the presence of dynamic and measurement noise is shown in Table 5.4. Accuracy was defined as the percentage of series that were correctly identified as measurement noise (decreasing cost function of SSVAR) and dynamic noise (non-decreasing cost function of SSVAR).

TABLE 5.4. NOISE IDENTIFICATION ACCURACY FOR CHAOS MAPS.

Map	Dynamic Noise	Measurement Noise	Accuracy (%)
Logistic	X		99.95
Logistic		X	96.88
Hénon	X		99.80
Hénon		X	100
Ikeda	X		36.40
Ikeda		X	89.14
Lorenz	X		69.33
Lorenz		X	50
Mackey-Glass	X		-
Mackey-Glass		X	88.88

5.2 Algorithm Applications and Limitations

Detection of measurement noise as a decrease in the cost function of SSVAR imposes various limitations on the use of the algorithm. Primarily, the series needs to be chaotic for nonlinear VAR to fit the data better than the linear fit. Series with negative Lyapunov exponents cannot be analyzed since the noise limit will always be zero. In addition, the decrease of the cost function requires SSVAR to iterate such that series where convergence is reached after the first iteration cannot be analyzed. These limitations of the noise identification algorithm prevent the application of the algorithm in all the tested chaotic maps. Therefore, nonchaotic series with measurement noise cannot be analyzed since, contrary to dynamic noise, the addition of measurement noise does not push the series into the chaotic attractor. The series for which noise distinction could not be run are represented by the asterisks in Figure 5.1.

The logistic map and the Hénon map, both of which are of the Volterra form, yield consistently accurate results for both dynamic and measurement noise. However, noise in discrete maps and continuous maps of the non-Volterra form was not as accurately identified. In the case of the Ikeda map, a discrete map

involving sinusoidal elements, the cost function of SSVAR constantly decreased even in the presence of dynamic noise. Though measurement noise yielded more accurate results than dynamic noise in this map, the results were still worse than those achieved with the logistic and Hénon maps. The Lorenz map and the Mackey-Glass equations yielded consistently decreasing cost functions in the presence of measurement noise, such that series with measurement noise were mostly correctly identified. However, the accuracy of the algorithm in the Lorenz map was greatly decreased in the presence of dynamic noise. The addition of dynamic noise to the Mackey-Glass equations caused SSVAR in all the created series to converge in one iteration, such that the algorithm could not be tested under the specified conditions. Therefore, the limitations of the proposed algorithm for distinguishing stochastic dynamic noise from measurement noise are such that they outweigh the benefits for applications to physiological data such as the beat-to-beat series. Though the algorithm's application is most beneficial in series with an underlying polynomial form, the concept and insights from this study can lead to more sophisticated measures for system identification.

5.3 Future Algorithms for Noise Discrimination in the Presence of Chaos

Noise discrimination with the SSVAR algorithm centers on estimating a signal with a dynamic noise term in the approximation and iteratively ridding the approximation of the dynamic noise, such that only measurement noise is represented in the output. Several limitations of the algorithm were presented in the previous section, suggesting critical improvements could dramatically increase the testability and accuracy of the algorithm. In addition, an improved algorithm can result in better approximation of the signal dynamics with SSVAR such that a modeling solution can be introduced in addition to the noise identification solution. An improvement on noise identification with SSVAR can be achieved by changing the modeling error correction (MEC), threshold, or estimation of the Volterra series coefficients. Determination of the modeling error correction, which determines what percentage of the approximated series is kept for further iterations, contains the challenge of subtracting the measurement error while keeping the underlying dynamics. A variable MEC could account for this challenge, where the signal-to-noise ratio of the observed series is approximated such that the MEC would be larger for iterations with smaller signal-to-noise ratios. The threshold can also be changed on a per-iteration basis to avoid the problem of the approximated series collapsing to zero. An alternate threshold determination algorithm starts with a very low threshold (~1%) to ensure iterations in SSVAR, the threshold is then increased at

each iteration up to a certain amount (~10%); finally, the algorithm stops iterating when convergence is reached, an initially decreasing cost function begins to increase, or the maximum number of iterations is reached. The most substantial improvement on the current SSVAR algorithm would be a more accurate representation of the Volterra series. In this study, the degree and order of the Volterra series had to be predefined, where values of 3 and 6 required the computation of 83 terms in the Volterra series. The application of Korenberg's fast orthogonal search (FOS) algorithm [34] for the determination of the Volterra coefficients would reduce the necessary number of computations by effectively selecting the largest Volterra coefficients such that more complex nonlinearities could be better represented. As a further extension, the implementation of the extension to the FOS algorithm [35] includes a dynamic noise term, and the estimate of this term in combination with the SSVAR algorithm could lead to more accurate system noise identification.

Part II

Risk Stratification of Mortality in Mild to Moderate Heart Failure by Heart Rate Variability Analysis

Chapter 6 Congestive Heart Failure and Heart Rate Variability

6.1 Congestive Heart Failure

Congestive heart failure (CHF), the common end of various diseases such as coronary artery disease and congenital heart disease, is typically characterized by the inability of the heart to pump enough blood to the body. Though the main anomaly of CHF is depressed ventricular function, a degenerative cycle aids the progression of the disease. Decreased cardiac output leads to enlargement of the cardiac chambers, which requires sympathetic activation to control the blood pressure. The sympathetic activation leads to vasoconstriction, and, in advanced stages of the disease, excessive vasoconstriction further impedes cardiac outflow. Treatments for CHF include diuretics to reduce pulmonary congestion and edema, digitalis to enhance myocardial contractility, vasodilators and angiotensin converting enzyme (ACE) inhibitors to counteract the vasoconstriction, and beta-adrenergic blockers to counter the sympathetic activation [36, 37].

Increasing supranormal sympathetic activity and subnormal parasympathetic activity accompany the progression of congestive heart failure [38-40]. In addition, CHF patients exhibit respiratory modulation of sympathetic outflow, but not of vagal outflow [40]. The sympathetic activation in CHF is probably caused by impaired baroreflex control in both mild and severe heart failure. However, the sympathetic activation in mild CHF differs from that in severe CHF, where the severe CHF patients have exhibited increased plasma norepinephrine where the mild CHF patients have not [39].

Two kinds of death commonly accompany CHF: sudden cardiac death and death from progressive pump failure. Pump failure death often occurs after progressive worsening of the CHF symptoms whereas sudden death implies a fatal electrical event (arrhythmic event) taking place during a time of clinical stability and is typically a manifestation of reduced left ventricular function [8, 9]. Sudden cardiac death can occur for a variety of reasons such as arrhythmia, acute myocardial ischemia, neurohumoral changes, and genetic predisposition. Though ventricular tachycardia becoming ventricular fibrillation is a major

cause of sudden death, the most effective treatments for decrease of sudden death have been non-antiarrhythmic drugs and internal cardiac defibrillators (for high-risk patients) [41].

6.2 Heart Rate Variability

6.2.1 Physiological Interpretation of Heart Rate Variability

Analysis of heart rate variability (HRV), the fluctuations in the beat-to-beat intervals, has been widely used for screening and characterization of diseases. Heart rate variability has proven to be a non-invasive, inexpensive index of the regulation of the autonomic system. Short and long-term oscillations in heart rate are modulated by the efferent vagal and sympathetic inputs to the sinus node. Autonomic function or dysfunction can be measured by the changes in HRV due to invasive techniques such as pharmacological testing and sympathetic microneurography, or more typically, non-invasive techniques such as posture changes, controlled respiration, and numerical analysis [42]. The effects of autonomic control experiments have been well studied in the analysis of HRV in the time and frequency domains. The time-domain measures pNN50 (percentage of normal-to-normal intervals greater than 50 ms) and RMSSD (the square root of the mean of the sum of squares of differences between adjacent NN intervals) correspond to parasympathetic activity while SDNN (the standard deviation of all NN intervals) is a measure of neurohumoral activation [43-45]. In spectral analysis, the high-frequency (HF) component reflects the efferent vagal activity and is thus synchronized to the respiratory rhythms [46]. However, the interpretation of the low-frequency (LF) component of HRV has been a controversial topic. An increase in the low-frequency power is attributed by some to an increase in the sympathetic activity and by others to a combination of sympathetic and parasympathetic activity [44, 46, 47]. Though the interpretation of the low-frequency component is debatable, it is agreed that the low-frequency to high-frequency power ratio (LF/HF) reflects sympathovagal balance [47]. Sympathovagal balance can also be evaluated from detrended fluctuation analysis (DFA), where a stronger short-term fractal correlation occurs for reciprocal variations in the sympathetic and vagal activity whereas the fractal organization of HRV breaks down for increases of both sympathetic and vagal activity [48]. The entropy of HRV has been shown to correspond to changes in the plasma concentrations of norepinephrine and dopamine [49]. Changes in any of these parameters can be explained by the autonomic imbalance that is characteristic of CHF, where subjects

with CHF exhibit sympathetic overactivity, baroreflex desensitization, and greatly depressed parasympathetic activity [40, 50, 51].

6.2.2 Nonlinearities in Heart Rate Variability

The nonstationary nature of the heart rate prevents analysis measures, particularly linear interpretations, from being applied to long segments of data. HRV is better characterized by nonlinear analyses due to influences by other physiological rhythms such as respiration or small perturbations in the heart. In 1985 Goldberger *et. al.* identified the fractal nature of the beat to beat intervals associated with healthy electrophysiological dynamics in the heart [52]. Chaos detection and nonlinear analyses such as detrended fluctuation analysis are able to better characterize complexities in heart rate, such as fluctuations in patients with decreased HRV where linear characteristics are not detectable [53]. Ivanov *et. al.* suggested the strong multifractality in heart rates of healthy patients indicates heart rate is controlled by several systems acting in feedback loops not in equilibrium [54]. However, others criticize the use of multifractal analysis on HRV arguing it assumes a deterministic nature of the signal whereas HRV is considered to have both deterministic and stochastic components [49]. Though many physiological systems exhibit irregular dynamics due to their complexity (which can be described by their fractal nature), it should be noted that fractal analysis is limited by the requirement of extensive data in order to minimize approximation errors [55].

6.2.3 Heart Rate Variability in Aging

The frequency components and complexity of HRV are modified with age, with several studies reporting decreased variance of beat-to-beat intervals for increasing age [47, 56, 57]. Aging is also associated with a decrease in the low frequency and high frequency components of HRV [57, 58]. This decrease corresponds to the reflection of the autonomic nervous system in the frequency components, where the spectral power measures the degree of autonomic modulations rather than changes in autonomic tone [44]. A comparison of the heart rate variability of different age groups and the changes in frequency for the supine and standing positions suggested different evolution for the changes in the β-adrenergic and parasympathetic modulations of heart rate with age [57]. Entropy analyses have also found HRV to vary with age, where elderly

subjects have a significantly lower approximate dimension and mean entropy than young adults [56, 58]. Similar results were found for different positions and respiration controls, such that the decreases can be attributed to age and its effect on cardiac control [56]. The relationship between age and decreasing HRV nonlinearities has also been evident with the correlation dimension, lyapunov exponent, $1/f$ slope, and detrended fluctuation analysis results [58].

6.2.4 Applications of Heart Rate Variability

Analysis of HRV has proven successful in characterizing cardiac and non-cardiac diseases as well as in risk stratification for death of patients with certain pathologies such as ischemic heart disease, myocardial infarctions, and congestive heart failure. A decrease in HRV has been reported for several pathologies such as myocardial infarction, diabetic neuropathy, cardiac transplantation, myocardial dysfunction, and tetraplegia [44]. In patients with ischemic heart disease, HRV analysis revealed a blunted circadian rhythm, sympathetic predominance after the onset of symptoms, and decreased beat-to-beat standard deviation as an independent predictor of death [47]. In screening for sleep apnea, pediatric subjects with obstructive sleep apnea syndrome (OSAS) exhibited higher heart rate chaos than healthy subjects whereas the severe OSAS subjects were also characterized with a higher low frequency to high frequency ratio than the subjects with mild or no disease [59, 60].

6.3 Previous Studies for Characterization of CHF and Mortality Prediction

6.3.1 Differences in HRV of normal and CHF subjects

The use of heart rate variability to characterize CHF and stratify the risk of death in different levels of the disease has been of great interest in recent decades. In 1988, Saul *et. al.* [61] analyzed the spectral components of healthy subjects and subjects with New York Heart Association (NYHA) class III-IV heart failure. They identified all the spectral components to be reduced in CHF (using slightly different definitions than those established in [44]), where the low frequency to high frequency ratio was not found to be significantly different between the two groups. The depression of LF along with loss of the circadian variations of the frequency components was reaffirmed in later studies [62-65]. Some studies have also found increased HF component in CHF, where the disagreement between reduction [61, 65] or increase [62, 64] of the HF power may arise from the discrepancy in severity of CHF. Other types of analysis have

also yielded differences between CHF and healthy subjects. Fractal analysis resulted in a steeper $1/f$ slope for the diseased subjects [62, 64] and Poincare plots changed their form with CHF [64], while the complexity of the heart rate was reduced in CHF during nighttime as measured by approximate entropy [63, 64] due to a loss of circadian rhythm of the parameter. Additionally, chaos analysis by means of nonlinearity detection with the Volterra autoregressive model identified the healthy heart rate as nonlinear more frequently than that of the CHF subjects, providing sufficient proof of a lower mean chaos level in CHF [66].

6.3.2 The United Kingdom Heart Failure Evaluation and Assessment Risk Trial (UK-HEART) Results

In the original UK-HEART publication, Nolan *et. al.* found mortality in CHF to be associated with decreased SDNN (<100 ms), pNN50, and RMSSD in univariate models, where the former reflects global heart rate variability and the latter two reflect a reduction in vagal activity [67]. A multivariate model of mortality which included clinical factors only retained SDNN from the HRV measures, and included cardiothoracic ratio, left ventricular end-systolic diameter, and sodium level as significant predictors. The second publication included frequency-domain analysis for the first 5 minutes of each hour and assigned points for each analyzed variable to determine the risk of mortality [43]. However, once again, SDNN remained the only HRV parameter that significantly predicted death in the multivariate model. Later studies found death to be more common in subjects with long QRS duration (> 150 ms) [68] or with impaired ventricular systolic function (< 50% ejection fraction) [69]. Risk of sudden death was not significantly determined by any time- or frequency-domain parameters in the CHF population, but rather by characterization of certain clinical parameters significant in determining the risk for all-cause mortality [70]. Analysis of time-domain (SDNN) and frequency-domain (VLF, LF, HF, total power) indices in combination with chemical and physiological factors yielded only low SDNN, low serum sodium, and high serum creatinine to be independent predictors of death from progressive heart failure [71].

6.3.3 Other CHF Mortality Studies

Linear and nonlinear analysis of HRV provides a non-invasive, inexpensive method to detect autonomic changes and aid the physician's treatment of the condition. Indices of HRV, individually or combined with physiological and chemical factors have previously been able to determine the risk of death as well

as the risk of sudden cardiac death or death from progressive pump failure [10, 72]. Results of previous studies rely heavily on the advancement of the disease in the subject group as well as the number of subjects included in the study such that studies often present contradictory results. In mild to severe CHF subjects, time-domain indices of total HRV (standard deviation of all normal-to-normal (NN) intervals) and the short-term component of HRV (percentage of NN intervals larger than 50 ms) have been shown to be significant univariate predictors of mortality [45, 62, 67, 73-75]. The significance of frequency-domain components such as very-low-, low-, and high-frequency, is not as well-established, since the significant univariate HRV indices vary with different studies; however, studies with significant absolute frequency-domain predictors included severe CHF subjects in the population [62, 73, 75, 76].

Nonlinear indices, though not as widely studied, have proven to be significant in various studies. Brouwer determined Poincare plots to be a significant predictor of mortality when time- and frequency-domain indices were not [77]. The abnormal Poincare plots, which were also described in [64], do not disperse with increasing RR interval but are rather classified as narrow when there was no increase in RR interval dispersion or complex when the RR intervals were in a cluster. The authors attributed the lack of prediction power of the linear indices to the lower stages of the disease. Other univariate predictors include the $1/f$ slope[62], detrended fluctuation analysis index [76], and short-term fractal exponent [78]. The significance of entropy in survival analysis for CHF has not been established since Ho found approximate entropy to not be a predictor of mortality [76] whereas the MUSIC study found CHF survivors to have significantly higher sample entropy [79].

Though many studies identified HRV indices as univariate predictors of mortality, many were not significant predictors in a multivariate model with chemical and other physiological data [10, 62, 67, 75]. The DIAMOND Study Group reached different conclusions from the UK-HEART study, where the differences were attributed to a higher mortality rate and more impared left ventricular function in the DIAMOND-CHF population [78]. The findings showed that though some linear and nonlinear HRV measures (standard deviation, very low frequency, mean heart rate, short-term fractal exponent) were able to predict mortality in a univariate model, when combined with clinical variables, only the short-term fractal scaling exponent could independently predict death.

Other studies have focused on predictors of sudden death or death from progressive pump failure. Szabo *et. al.* included NYHA class II-IV subjects in their study and determined frequency indices to only determine the risk for progressive pump failure death whereas SDNN and pNN50, markers of vagal tone, were independent predictors of mortality [45]. Galinier *et. al.* found several significant predictors of mortality, whereas a decrease in the standard deviation of normal-to-normal beat intervals (SDNN) and a lower daytime low frequency component were independent predictors for progressive pump failure death and sudden death respectively [73]. Guzzetti *et. al.* determined many HRV measures to be univariate predictors of progressive pump failure death, whereas when combined with clinical variables, the very low frequency component was the only HRV measure that independently predicted pump failure death in the multivariate model [80]. Low frequency power was a predictor for sudden death, yet the multivariate model indicated the same information could be provided by the VLF component. In addition, La Rovere *et. al.* found the LF component was an independent predictor of sudden death in a short-term controlled breathing experiment [81]. Due to the length of the recording, the VLF component was not analyzed, such that Guzzetti's redundancy conclusion could not be proved or disproved.

Chapter 7 Data and Experimental Methods

7.1 Congestive Heart Failure Data

7.1.1 Data Acquisition for UK-HEART [43, 67-70]

The data for this study are those used in the United Kingdom heart failure evaluation and assessment of risk trial (UK-HEART). The UK-HEART studies were carried out in agreement with the principles outlined in the Declaration of Helsinki with written consent for all the patients. The data were gathered in 8 hospitals across the United Kingdom, where 18-85 year-old outpatients with symptoms of CHF for at least three months were recruited between April 1993 and December 1995. Patients were in New York Heart Association (NYHA) functional class I-III and had evidence of cardiac dysfunction at rest such as pulmonary venous congestion, pulmonary edema or cardiothoracic ratio >0.55 on at least one chest radiograph, or a documented radionuclide or echocardiographic ejection fraction <45%. The exclusion criteria for patients included conditions that independently impaired autonomic function, documented constrictive or hypertrophic cardiomyopathy, sustained non-sinus dysrrhythmias, atrioventricular conduction defects, or a noncardiac disease likely to limit survival.

Clinical measurements were made for each patient in the form of a posteroanterior chest radiograph, venous blood sample and two-dimensional and M-mode echocardiograph. Twelve-lead electrocardiograms were also recorded in a clinical setting and analyzed by a senior cardiologist blinded to the patient's characteristics. A twenty-four hour ambulatory electrocardiogram was recorded (Tracker, Reynolds Medical Ltd) during normal activity. These recordings were analyzed with a Pathfinder system by a technical staff blinded to patient characteristics in order to perform arrhythmia analysis, whose presence could affect the outcome of CHF, and extract the normal-to-normal RR intervals. Recordings were rejected if they were less than 16 hours in duration or less than 90% of the recording could be analyzed.

7.1.2 Definition of Mode of Death [67, 68, 70]

The death certificates, autopsy findings, and general practitioners' records were reviewed by at least two senior physicians who classified the mode of death into one of four categories:

1. Sudden cardiac death – Death occurred within one hour of a change of symptoms or when the patient was sleeping and not monitored but had been previously stable.

2. Progressive pump failure – A documented period of symptoms or hemodynamic deterioration preceded death.

3. Other cardiovascular death – Death did not occur suddenly and was not associated with progressive heart failure.

4. Non-cardiovascular death.

7.1.3 Patient Group Characterization

The group characteristics for the patients are outlined in the following table as mean (standard deviation) or as percentage. Of the patients recruited for the UK-HEART studies, four-hundred and eight had data that could be analyzed of which 127 died in the five-year follow-up period. Of those who died, 48 suffered sudden cardiac death and 58 died from progressive pump failure.

TABLE 7.1. PATIENT GROUP CHARACTERISTICS.

Age	62.8 (0.41)
Men	75%
NYHA class I	3%
NYHA class II	60%
NYHA class III	36%
NYHA class IV	1%
Creatinine concentration	119 (2.1) μmol/l
Sodium concentration	140 (0.16) mmol/l
Ischaemic heart disease	7.7%
Non-sustained ventricular tachycardia	33%
Treatment:	
Angiotensin converting enzyme inhibitors	83%
Loop diuretics	97%
Digoxin	17%
Amiodarone	14%
Mean annual mortality	6.2%

7.2 Heart Rate Variability Analysis Indices

Only the normal-to-normal beat intervals (NN) were considered for the time-domain measures, whereas all beats were considered for the other HRV parameters.

7.2.1 Time-Domain Measures

The analysis included several traditional time-domain measures [44]: the standard deviation of all NN intervals (SDNN), the standard deviation of the averages of NN intervals for 5-minute segments in the complete recording (SDANN), the square root of the mean of the sum of squares of differences between adjacent NN intervals (RMSSD), and the percentage of adjacent intervals that differ by more than 50 ms (pNN50).

The calculation of SDNN over long periods of time, such as 24-hour data, encompasses short-term and long-term oscillations of the heart rate and is thus a measure of overall HRV. However, the value of SDNN can only be compared to that of other recordings of similar duration since the standard deviation is dependent on length and previous research has found standard deviation to increase with recording time [44, 46]. The SDANN characterizes the long-term components of the HRV whereas RMSSD and pNN50 estimate the short-term components of HRV. The high correlation of RMSSD and pNN50 along with the statistical properties of each measurement make RMSSD the more desirable estimation of the high-frequency component of HRV [44]. However, since pNN50 had been previously utilized as a prediction parameter with the UK-HEART database, it was included in this study [67].

7.2.2 Frequency-Domain

The total power (TP), very low frequency (VLF), low frequency (LF), and high frequency (HF) were measured in frequency-domain analysis. The RR series was divided into 12-minute segments for analysis, a duration that is long-enough time to capture the VLF component [44] while diminishing the nonstationary characteristic of the heart rate. Cubic spline interpolation at 4 Hz was performed on the data in each segment to achieve even sampling of the series. The power spectral density (PSD) was calculated by means of the widely-applied Welch's method [82, 83] of averaged modified periodograms. The algorithm divides the data segment into 8 sections of equal length overlapping by 50%. A Hamming

window is applied to each segment and the 1024-point discrete Fourier transform (by means of the Fast Fourier Transform method) of each windowed segment is calculated. The modified periodograms of each segment are then averaged to compute the power spectral density.

The range of the frequency components were calculated as designated by the Task Force of the European Society of Cardiology and the North American Society of Pacing and Electrophysiology [44]. The VLF component is the integrated PSD below 0.04 Hz, LF is defined as the power between 0.04 Hz and 0.15 Hz, and the HF component is calculated between 0.15 Hz and 0.4 Hz. The low frequency to high frequency ration (LF/HF) is the absolute LF divided by the absolute HF for each segment.

7.2.3 Entropy Measures

Entropy measures quantify the regularity of a series, such that the entropy of a series decreases with increasing predictability of the series' fluctuations. Approximate entropy was developed by Pincus [84] in 1991 as a measure of the system's complexity that did not require extensive amounts of data, whereas sample entropy is a more recent algorithm [85] that accounts for some of the singularities in the approximate entropy algorithm, providing a more accurate method of determining the degree of regularity in a series.

Approximate Entropy (ApEn) does not establish the presence of chaos, but rather distinguishes complex systems based on their parameters. The application of the algorithm extends to systems of varied dimensions, noise contamination levels (the tolerance parameter acts as a filter), and chaos intensities. In addition, it can quantify regularity in systems that exhibit solely stochastic or mixed, stochastic and deterministic, dynamics [84, 86]. ApEn reflects the logarithmic likelihood that two sequences that are similar (within a tolerance r) for m points remain similar on incremental comparisons. A time series that exhibits frequent and similar epochs has a relatively small ApEn value, reflecting a high degree of regularity; similarly, greater nonlinearities and stochastic influences increase the value of ApEn.

Given an N-point time series $x(n) = [x(1), x(2), ..., x(N)]$, m-vectors, $X(1)$ to $X(N\text{-}m\text{+}1)$ are defined by:

$$X(i) = [x(i), x(i+1), ..., x(i+m-1)] \qquad , i = 1, ..., N-m+1 \tag{7.1}$$

where m defines the length of comparison. The distance $d[X(i), X(j)]$ between vectors $X(i)$ and $X(j)$ is defined as the maximum absolute difference in their respective scalar components:

$$d[X(i), X(j)] = \max_{k=0,m-1} \left[\left| x(i+k) - x(j+k) \right| \right]. \tag{7.2}$$

Define $C_r^m(i)$, the prevalence of repetitive patterns of length m in the series, for $i = 1,\ldots,N\text{-}m\text{+}1$:

$$C_r^m(i) = \frac{V^m(i)}{N-m+1}, \tag{7.3}$$

where $V^m(i)$ is the number of $d[X(i), X(j)] \le r$ and r is the predefined tolerance for similarity. Since ApEn does not reflect linear likelihood, the logarithmic parameter is defined as:

$$\phi^m(r) = \frac{1}{N-m+1} \sum_{i=1}^{N-m+1} \ln(C_r^m(i)). \tag{7.4}$$

The ApEn value for a finite data length of N, patterns of length m, and similarity criterion r is then defined as:

$$ApEn(m, r, N) = \phi^m(r) - \phi^{m+1}(r). \tag{7.5}$$

Approximate entropy was calculated for each of the 12-minute RR series in the recording. The algorithm was implemented with $m = 2$ and $r = 20\%$ of the standard deviation of each segment.

Sample entropy improves on the ApEn algorithm by removing the dependence on the series length and avoiding counting self-matches. Thus, SampEn produces a more consistent and unbiased measure of series regularity [85]. The beginning of the algorithm's implementation is similar to that of ApEn, and the algorithms diverge in the calculation of the likelihoods and probabilities.

Given an N-point time series $x(n) = [x(1), x(2), \ldots, x(N)]$, m-vectors, $X(1)$ to $X(N\text{-}m\text{+}1)$ are defined by:

$$X(i) = [x(i), x(i+1), \ldots, x(i+m-1)] \qquad , i = 1,\ldots, N-m+1. \tag{7.6}$$

The distance $d[X(i), X(j)]$ between vectors $X(i)$ and $X(j)$ is defined as the maximum absolute difference in their respective scalar components:

$$d_m[X(i), X(j)] = \max_{k=0,m-1} \left[\left| x(i+k) - x(j+k) \right| \right]. \tag{7.7}$$

In order to avoid counting self-matches, $B^m(r)$ and $A^m(r)$ were defined as the probabilities that two sequences will match for m and $m+1$ points respectively. These probabilities were calculated by first determining $B_r^m(i)$ and $A_r^m(i)$ for all i=1, ...,N-m+1:

$$B_r^m(i) = \frac{V^m(i)}{N-m+1}, \tag{7.8}$$

where $V^m(i)$ = number of $d_m[X(i), X(j)] \leq r$ for $i \neq j$ and

$$A_r^m(i) = \frac{V^{m+1}(i)}{N-m+1}, \tag{7.9}$$

where $V^{m+1}(i)$ = number of $d_{m+1}[X(i), X(j)] \leq r$ for $i \neq j$. The probabilities are then calculated from these quantities:

$$B^m(r) = \frac{1}{N-m} \sum_{i=1}^{N-m} B_r^m(r) \tag{7.10}$$

$$A^m(r) = \frac{1}{N-m} \sum_{i=1}^{N-m} A_r^m(r). \tag{7.11}$$

The sample entropy of the signal is defined everywhere except when B=0 or A=0, which correspond to no detected regularity, where SampEn is assigned as 1. For all other values of A and B, SampEn is the negative natural logarithm that two sequences similar for m points remain similar for m+1 points:

$$SampEn(m, r, N) = -\ln\left(\frac{A^m(r)}{B^m(r)}\right). \tag{7.12}$$

Sample entropy was calculated for each of the 12-minute RR series in the recording. The algorithm was implemented with m = 2 and r = 20% of the standard deviation of each segment.

7.2.4 Detrended Fluctuation Analysis

Detrended fluctuation analysis (DFA), developed by Peng in 1994 [87], quantifies long-range power law correlations as well as mono-fractal scaling properties in a signal [87, 88] by means of a modified root mean square analysis of a random walk [89]. The scaling exponents are calculated such that the input signal is not limited to noise-free and stationary series, since apparent correlations due to non-stationarity

are not detected, but the series must be of extensive length. Thus, the DFA method is capable of distinguishing the underlying complex systems from the fluctuations caused by external stimuli [46].

The N-point RR series $x(n) = [x(1), x(2), ..., x(N)]$ is integrated as:

$$y(k) = \sum_{i=1}^{k} [x(i) - \mu_x], \tag{7.13}$$

where $x(i)$ is the ith data point and μ_x is the average RR interval calculated by:

$$\mu_x = \frac{1}{N} \sum_{i=1}^{N} x(i). \tag{7.14}$$

The integrated time series is divided into windows of equal length, n. In each window, a least-squares line is fit to the data to represent the local trend and is denoted $y_n(k)$. Next, the integrated time series $y(k)$ is detrended by subtracting the local trend, $y_n(k)$, in each window. The root-mean-square fluctuation of the integrated and detrended time series is calculated by:

$$F(n) = \sqrt{\frac{1}{N} \sum_{k=1}^{N} [y(k) - y_n(k)]^2}. \tag{7.15}$$

The computation is repeated over all time scales (window lengths) to characterize the relationship between $F(n)$, the average fluctuation, and the window length n.

Typically, $F(n)$ will increase with n. A power-law relation between $F(n)$ and n indicates the presence of scaling $F(n) \sim n^{\alpha}$. A linear relationship on a log-log plot indicates the presence of power law (fractal) scaling. Under such conditions the fluctuations can be characterized by the scaling exponent α, the slope of the line relating *log* $F(n)$ to *log* n. For $0<\alpha<0.5$, large and small values of the series alternate, $\alpha = 0.5$ is characteristic of white noise, $0.5<\alpha<1$ indicate persistent power-law correlations, and $\alpha>1$ exists for correlations that are not of the power-law form.

DFA was performed on the complete RR series, rather than to 12-minute intervals of data. In order to avoid bias in $F(n)$ caused by averaging of too few windows, the DFA algorithm was only implemented with $n \leq N/4$. The short-range (α_s) and long-range (α_l) correlations were computed for each individual. The slope for the entire recording (α) was also calculated, however, this DFA parameter is only accurate when α_s and α_l are similar.

7.2.5 Numerical Titration

Numerical titration (described in Section 2.2) was performed on 12-minute segments of the RR series. The two outputs of the algorithm, noise limit (NL) and nonlinearity detection rate (DR), were analyzed for prediction of mortality in CHF. The NL gives a relative measure of chaos intensity, whereas the DR indicates the persistence of chaos in the series. The DR was calculated as the percentage of nonlinear 12-minute segments in a 3-hour time window.

7.3 Statistical Methods

7.3.1 Receiver Operating Characteristic Curve Analysis

Receiver operating characteristic (ROC) curve analysis was performed to determine the best HRV indices for distinguishing the nonsurvivors from the survivors. In ROC analysis, the indices were incremented by a predetermined step (1 for absolute frequency values and 10^{-5} for all other parameters). The area under the ROC curve (AUC), sensitivity (Se), and specificity (Sp) were calculated for all indices. The AUC quantifies the goodness of test, where a perfect test for mortality has an AUC of 1 while a random test has an AUC of 0.5. The sensitivity is a measure of how well the event (death) was identified,

$$Se = \frac{True\ Positives}{True\ Positives + False\ Negatives}, \tag{7.16}$$

whereas the specificity quantifies how well the non-events (survival) were identified,

$$Sp = \frac{True\ Negatives}{False\ Positives + True\ Negatives}. \tag{7.17}$$

The critical value was defined as the index value which resulted in the lowest error, the point on the ROC curve closest to a sensitivity and specificity of one.

ROC analysis was performed on the training set (50 patients), where the determined critical HRV indices were tested for effectiveness in classifying the rest of the population (358 patients). ROC analysis was also performed on the entire CHF dataset (408 patients) in order to determine the critical values for the HRV indices, sensitivity, and specificity for the patient population.

7.3.2 Support Vector Machine Classification

Support vector machines (SVM) present a method for constructing classifiers in a high dimensional feature space such that they guarantee good predictive performance in the lower-dimensional parameter space [90, 91]. A linear function is constructed in the feature space as to minimize the error in the training data, where the linear decision function with maximal separation without error is defined as the optimal hyperplane [91, 92]. The margin between the two groups is constructed by the support vectors derived from the training set, and, in the case where the training set cannot be separated without error, the soft margin hyperplane is determined as to minimize the classification errors in the training set and separate the test set elements with maximal margin. The optimal separating hyperplane is determined by minimizing

$$\Phi(w,\xi)=\frac{1}{2}\|w\|^2+C\sum_i \xi_i \tag{7.18}$$

with respect to the vector w [92], where C is a given value and ξ is a measure of classification errors. In order to avoid the extensive computations in conversion to a high-dimensional feature space, the kernel function allows for similarity to dot products in the feature space from the input space. Many kernel functions exist for various data set properties. The Gaussian radial basis function (RBF) was implemented since it constructs both the centers and Lagrange multipliers necessary for the construction of the optimal hyperplane [90-92]. The RBF kernel is calculated as:

$$K(x,x')=\exp\left(-\frac{\|x-x'\|^2}{2\sigma^2}\right). \tag{7.19}$$

Support vector machine classification was implemented on the training set to determine classification rules between the survivors and nonsurvivors, where the determined boundaries were then applied to the test set. The Matlab code used to implement the classifiers was that developed by Dr. Gunn, and further explanations of SVM theory and the computation of the optimal hyperplane can be found in [92]. SVM was performed with combinations of 2 or 3 different HRV indices in order to complement the ROC analysis by determining the combination of indices that minimized classification errors in the test set.

7.3.3 Survival Analysis [93-95]

Survival analysis presents a tool for determining risk functions for different patient groups and identifying significant predictors of mortality. In survival analysis, the survival time is the time from the recording until death and the censoring time is the time until the subject withdraws from the study. The analysis implemented fixed type I right-censoring; such that survival time was not measured above the study length of 5 years, where time zero was defined as the time of the initial electrocardiogram recording. Survival and the risk of an event, in this case death, can be described by three main functions where the variable T describes time until an event and $F(t)$ is the cumulative distribution function of T:

1. The survival function $S(t)$ is the probability that an event occurs after time t:

$$S(t)=\Pr\{T>t\}=1-F(t). \tag{7.20}$$

2. The cumulative hazard function $\Lambda(t)$ describes the risk accumulated up until time t:

$$\Lambda(t)=-\log S(t). \tag{7.21}$$

3. The hazard function $\lambda(t)$ is used to describe the risk of an event, in this case death, for a small time interval given that the event has not occurred. The hazard function is described as:

$$\lambda(t)=\lim_{u\to 0}\frac{\Pr\{t<T\le t+u\,|\,T>t\}}{u}a. \tag{7.22}$$

The Kaplan-Meier product-limit estimator estimates the survival function when censored data is present. The attractiveness of the estimator arises from its lack of assumptions about the distribution, which is estimated as:

$$S_{KM}(t)=\prod_{i:t_i<t}\left(1-\frac{d_i}{n_i}\right), \tag{7.23}$$

where t_i are the ordered times of the events, d_i are the number of events at time t_i, and n_i is the number of subjects at risk (have not been censored or died just prior to t_i). In order to analyze independent events with different causes, such as sudden cardiac death and death due to progressive heart failure, events that did not occur by the cause of interest were censored.

The Cox proportional hazards model was used as a tool for determining which HRV indices were significant univariate and multivariate predictors of death. The semiparametric nature of the Cox

proportional hazards model contributes largely to its popularity in survival analysis. Contrary to the exponential and Weibull models, the Cox model makes no assumptions about the hazard function; thus the regression parameters can be estimated without estimating the baseline hazard funtion. However, the regressors are assumed to act multiplicatively and are thus linearly related to the log hazard function. In addition, the model assumes that the effect of the predictors on the hazard function does not change with time, such that even though the number of events (deaths) increases with time in groups with high and low parameter values, the hazard ratio does not vary with time. The hazard ratio can be interpreted as a relative risk, where a hazard ratio of 0.5 indicates the relative risk of death of one group is half that of the other group [96]. The Cox proportional hazards model has been shown to be as effective as parametric models for which the assumptions are satisfied and more effective than the parametric models with equivocal assumptions.

The proportional hazards model is described as:

$$\lambda(t \mid X) = \lambda(t)\exp(X\beta), \tag{7.24}$$

where X={X1, X2, X3, ..., X_k} are the predictor variables. The terms Xβ can be isolated as:

$$\log \lambda(t \mid X) = \log \lambda(t) + X\beta. \tag{7.25}$$

Thus β_j can be interpreted as the increase in log hazard when X_j is increased by one unit while keeping all other predictors constant. In parametric models, these parameters are estimated by means of the maximum likelihood estimator (MLE). In the Cox model, as long as there are no objects with the same failure time, the log partial likelihood is calculated as:

$$\log L(\beta) = \sum_{Y_i\, uncensored} \left\{ X_i\beta - \log\left[\sum_{Y_j \geq Y_i} \exp(X_j\beta) \right] \right\}. \tag{7.26}$$

The significance of the parameters in the univariate or multivariate models are assessed by means of a chi-square test. The results of the Cox model are assessed by means of the significance of the variables as event predictors and the hazard ratio.

Chapter 8 Training Set and Test Set Results

8.1 Results for Training Set

8.1.1 ROC Analysis

In ROC analysis, the test accuracy is determined by the point closest to a sensitivity (Se) and specificity (Sp) of 1 while the area under the curve (AUC) reflects the goodness of the test. For some variables, mainly noise limit and nonlinearity detection rate, the 8am-8pm (day) portion of the variable is the best discriminator between the subjects who died and the survivors. This trend results from the different circadian rhythms of the survivors and nonsurvivors. For the NL and DR, the survivors have a stronger circadian rhythm, and since the survivors have a lower mean index the circadian rhythm causes the two groups to have more similar values during the nighttime. Other variables, such as LF/HF yielded accurate detectors for all three time segments, where circadian rhythms were either not reflected or enlarged the difference at night. The progression of average values of NL and LF/HF can be seen in Figure 8.1.

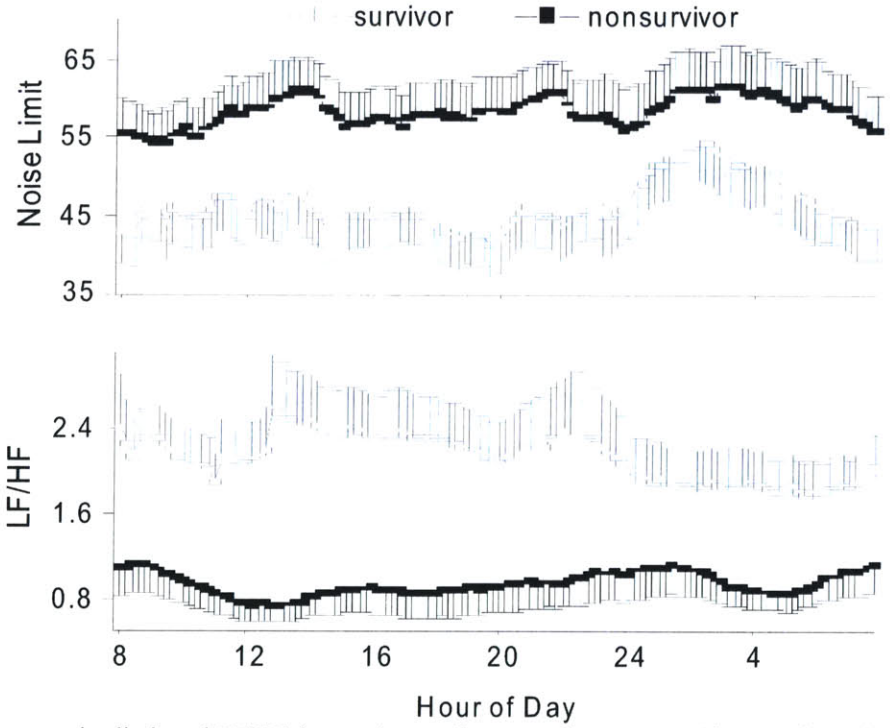

Figure 8.1. Average noise limit and LF/HF for survivor and non-survivor group. The error bars show the standard error for each segment. The values for each 12-minute segment were averaged over 3-hours to yield smooth curves.

The five largest AUC corresponded to the day LF/HF(.778), α_s (0.747), 24-hour LF/HF (0.742), day DR (0.731), and 24-hour DR (0.726). The HRV indices with highest detection accuracy are listed in Table 8.1.

TABLE 8.1. INDICES WITH HIGHEST ACCURACY IN ROC ANALYSIS

Index	AUC	Se (%)	Sp (%)	Critical Value
NL (day) *	0.70	77.27	75.00	50.90
LF/HF (day)	0.78	71.43	77.27	1.20
LF/HF (24 h)	0.74	67.86	72.72	1.06
LF/HF (night)	0.72	67.86	72.72	0.99
NL (24 h) *	0.69	72.72	67.86	53.59
α_l	0.64	85.71	59.09	0.89
NL (night) *	0.66	77.27	60.71	47.49
α_s	0.75	92.86	54.55	0.49
SampEn (24 h)	0.68	78.57	59.09	0.87
SampEn (day)	0.67	85.71	54.55	0.79

* Has higher value for the nonsurvivor group.

Figure 8.2 plots the area under the ROC curve for the chaos, DFA, time-domain, entropy, and frequency-domain analysis variables. In addition, the ranking of the AUC of a particular variable with respect to all other variables is indicated by the number on top of each bar. Most variables were calculated over the 24 hours, daytime (8am-8pm) and nighttime (8pm-8am) such that redundant information is provided by each time division but the circadian rhythms of the variables are utilized to maximize the detection rate. In addition, redundant information is provided by ApEn and SampEn since both measure regularity in the signal, and some time- and frequency-domain measures.

Total power (TP) and RMSSD resulted the worst detection variables, where the AUC for TP during the day was 0.539, such that the detection was almost carried out in a random fashion whereas the detection with RMSSD (AUC = 0.5) can be classified as random.

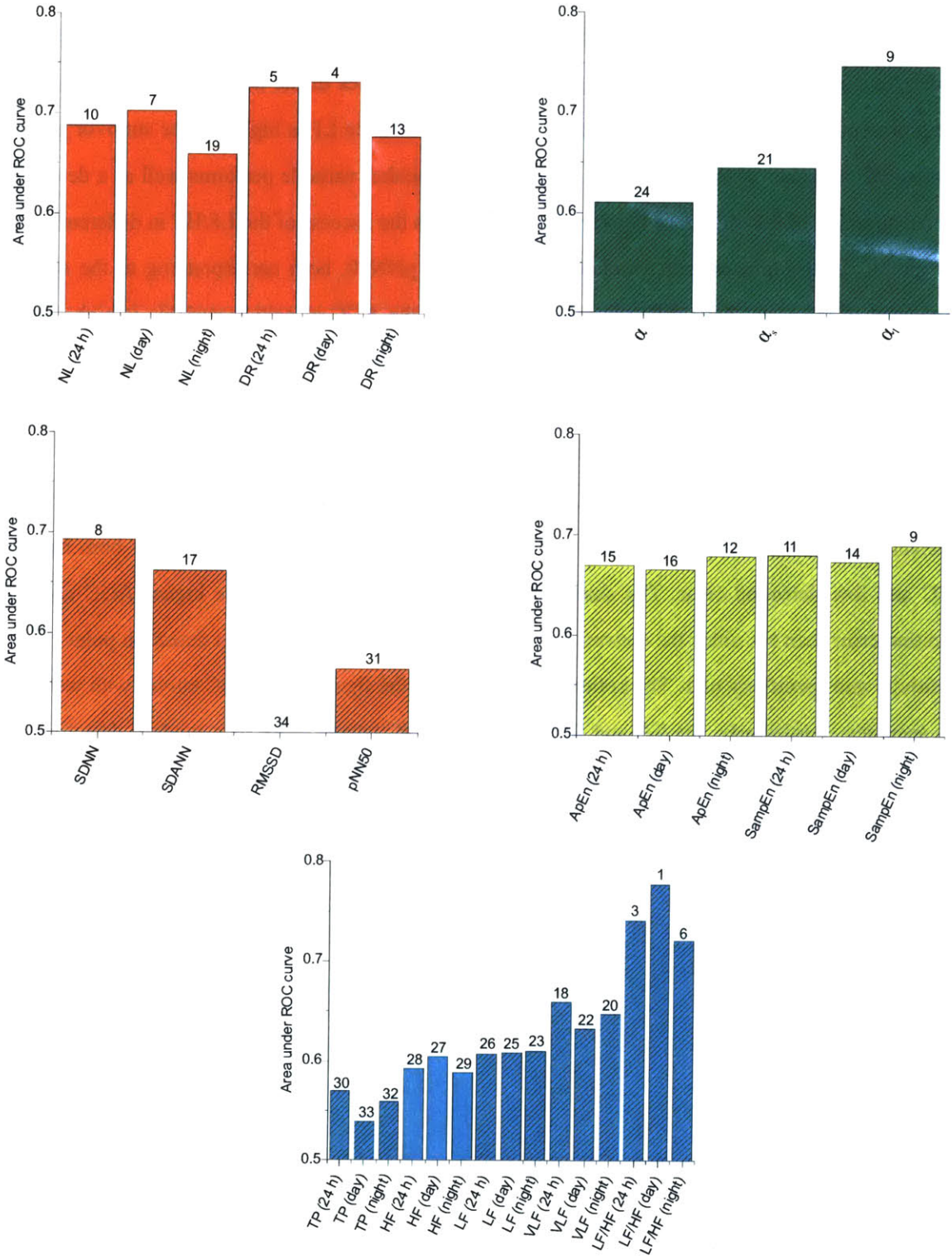

Figure 8.2. Results of ROC analysis. The bar graphs plot the area under the ROC curves. The shaded bars represent higher values for the survivors while solid bars represent lower values for the survivors. The ranking of the AUC for each parameter is written on top of each bar.

The sign of the difference of the variable between the dead and survivor groups corresponds to the bar shading in Figure 8.2, where solid bars represent larger variables in the nonsurvivor group and shaded bars represent larger variables in the survivor group. The absolute LF is higher in the survivor group and absolute HF is higher in the nonsurvivor group. Though neither variable performs well as a detector, the inverse direction of the difference between groups explains the success of the LF/HF in differentiating the two groups. In the time-domain variables, RMSSD and pNN50, both corresponding to the short-term component of the series have different shadings. Though the AUC of neither variable is high enough to qualify as an accurate detection variable, RMSSD and HF are both higher in the survivor group, reinforcing the idea that RMSSD is a better estimate of high frequency than pNN50 [44].

Six ROC curves are plotted in Figure 8.3, illustrating how the different shapes of the curves generate different results for AUC and detection accuracy. The LF/HF and NL during the day both have large AUC and low detection error. The shape of the day DR curve explains the higher AUC and higher detection error than NL since the convex property of the ROC curve prevents a detection point close to a sensitivity and specificity of 1. The bottom three graphs in the figure show ROC curves with worse AUC and accuracy. Particularly, the TP and RMSSD show ROC curves close to a random detection where almost every time the sensitivity increases, the specificity decreases resulting in a graph that closely follows a line with unity slope.

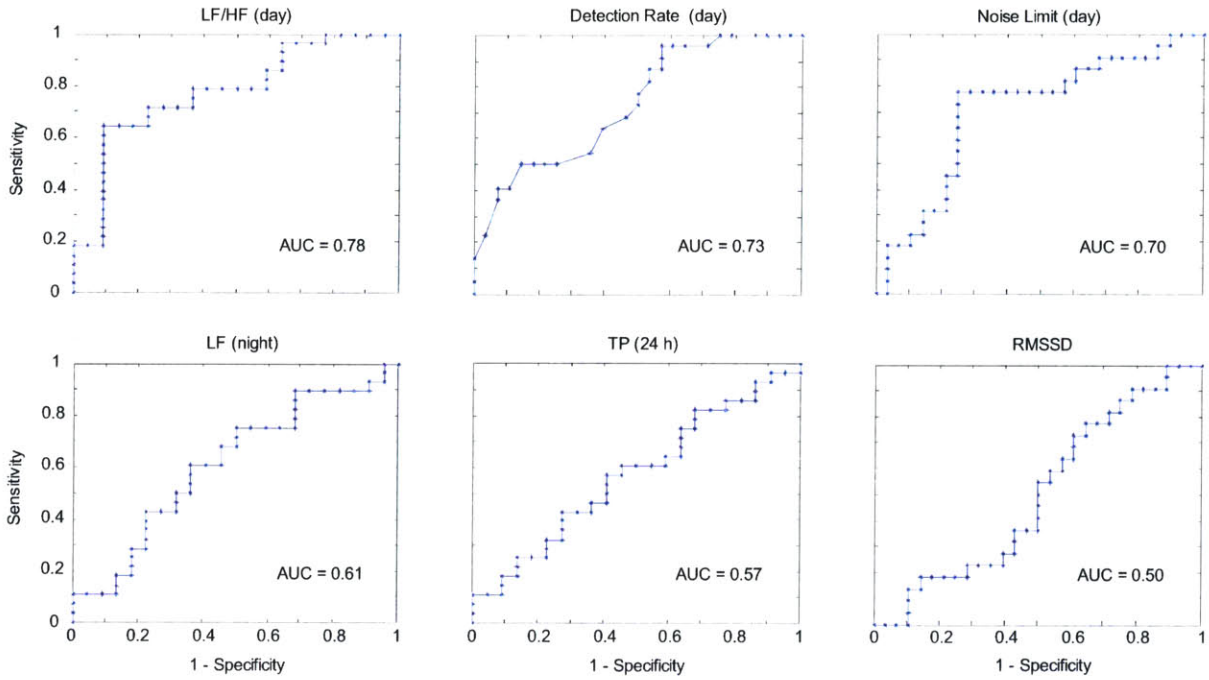

Figure 8.3. ROC curves for accurate and random-like mortality detectors.

8.1.2 Cox Proportional Hazards Analysis of Training Set

Cox proportional hazards analysis determines which HRV indices were univariate and multivariate predictors of all-cause mortality. The α index in DFA was not included in any of the Cox hazards analyses due to the requirement of similar short-range and long-range exponents which limits the applicability of the index. The results for the univariate significant (p value < 0.05) and marginally significant (p value < 0.10) HRV indices are shown in Table 8.2. HRV indices with a blank multivariate p value were eliminated from the multivariate model in the backwards selection of parameters. The logarithm of the hazard ratio is positive for HRV indices which are higher in those with a higher risk of mortality, where if the log is near zero both groups (survivors and nonsurvivors) have similar risk of mortality. The χ^2 and p value are the statistical results which indicate the significance of each predictor. The most significant univariate predictors were entered in the multivariate model, where several measures of NL, LF/HF, DR, SampEn, and VLF were independent predictors of mortality.

TABLE 8.2. PROPORTIONAL HAZARDS RESULTS FOR SIGNIFICANT UNIVARIATE AND MULTIVARIATE PREDICTORS.

Index	Log of Univariate Hazard Ratio	Univariate χ^2	Univariate P value	Multivariate P value
α_s	-0.9272	8.29	0.0040	
LF/HF (day)	-0.2959	7.42	0.0065	0.0050
DR (day)	1.5971	7.11	0.0076	0.0015
LF/HF (24 h)	-0.2792	6.71	0.0096	0.0052
SDNN	-7.4243	6.34	0.0118	0.1087
SampEn (night)	-0.8140	6.32	0.0119	0.0150
DR (24 h)	1.6447	6.08	0.0137	0.0058
SampEn (24 h)	-0.8894	5.82	0.0159	0.0201
NL (day)	0.0105	5.76	0.0164	0.0547
SDANN	-7.3466	5.60	0.0179	0.2657
ApEn (night)	-1.0701	5.60	0.0179	
LF/HF (night)	-0.2396	5.21	0.0224	0.0050
SampEn (day)	-0.8074	4.38	0.0363	
NL (24 h)	0.0093	4.20	0.0404	0.0219
VLF (24 h)	-0.0003	3.95	0.0470	0.0361
VLF (night)	-0.0003	3.88	0.0488	0.0716
DR (night)	1.1650	3.78	0.0517	
ApEn (day)	-0.9541	3.61	0.0573	
α_l	-0.6722	3.15	0.0760	
NL (night)	0.0072	3.02	0.0825	0.0219

Kaplan-Meier curves for several HRV indices are plotted in Figure 8.4. The left panel plots the most significant mortality predictors (NL and LF/HF) whereas less significant and not significant indices are plotted in the right panel. It can be seen from the figure that the NL (day) and LF/HF (day) yield the largest difference in Kaplan-Meier curves for the low-risk and high-risk groups. The critical values for the division into 2 groups were those determined by the ROC analysis.

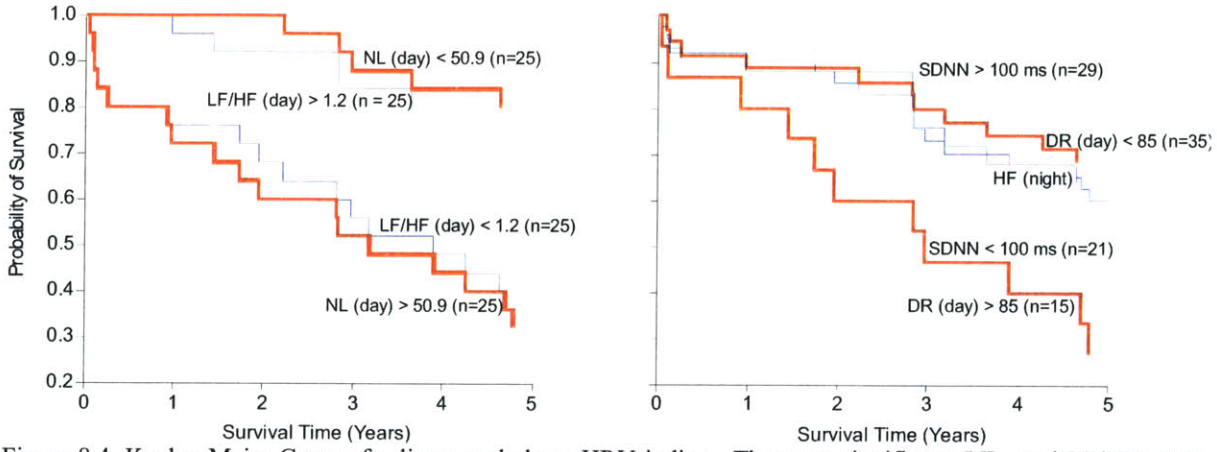

Figure 8.4. Kaplan Meier Curves for linear and chaos HRV indices. The most significant (NL and LF/HF) HRV indices are plotted in the left graph. The right graph illustrates the Kaplan Meier curve for the classic SDNN, the newer nonlinearity detection rate index, and the not-significant high frequency. The blue HF curves are for the cutoff value of 478 ms^2 where 25 of 50 subjects were above the cutoff value.

8.2 Analysis of Test Set

8.2.1 ROC Analysis with Training Set Parameters

The critical values derived from ROC analysis of the training set (Section 8.1.1) were examined as detectors on the test set (n=358). However, the sensitivity and specificity were greatly decreased in the test set, suggesting the training set did not contain a representative sample of all HRV indices in the population. In the test set, noise limit was no longer an accurate predictor of mortality. The best predictors were LF/HF (day) and α_s, both of which had much larger error in the test set than in the training set. The test set sensitivity and specificity of the ten HRV indices with highest accuracy in the training set (Table 8.1) are listed in Table 8.3.

TABLE 8.3. ROC RESULTS FOR TEST SET.

Index	Se (%)	Sp (%)	Errors	Accuracy (%)
NL (day)	41.67	39.92	213	40.17
LF/HF (day)	69.17	61.77	128	64.04
LF/HF (24 h)	60.00	67.65	125	64.89
LF/HF (night)	63.33	65.97	125	64.89
NL (24 h)	37.50	39.92	218	38.76
α_l	43.33	65.97	149	58.15
NL (night)	26.67	47.48	213	40.17
α_s	69.17	61.35	129	63.76
SampEn (24 h)	63.33	46.64	171	51.97
SampEn (day)	55.00	56.72	157	55.90

8.2.2 Support Vector Machine Classification

Support vector machine classification (SVC) yielded boundaries in a 2-dimensional and 3-dimensional space that accurately distinguished survivors from nonsurvivors in the training set. Detection of mortality in the test set from the training set boundaries yielded fewer errors than traditional ROC analysis (Section 8.2.1) for certain combinations of HRV indices. A total of 20 combinations of two HRV indices yielded fewer than 125 errors (minimum error achieved by ROC analysis) in the test set, where the errors for the most accurate combinations are plotted in Figure 8.5. The five 2-dimensional combinations that resulted in the fewest errors were: 24-hour NL and 24-hour LF/HF, 24-hour NL and day LF/HF, 24-hour NL and night LF/HF, night DR and SDNN, and night DR and SDANN. Thus, best detection was achieved through combinations of a chaos index (NL, DR) and a linear index (LF/HF, SDNN, SDANN). The complete results for the ten HRV index combinations that yielded the fewest errors are presented in Table 8.4.

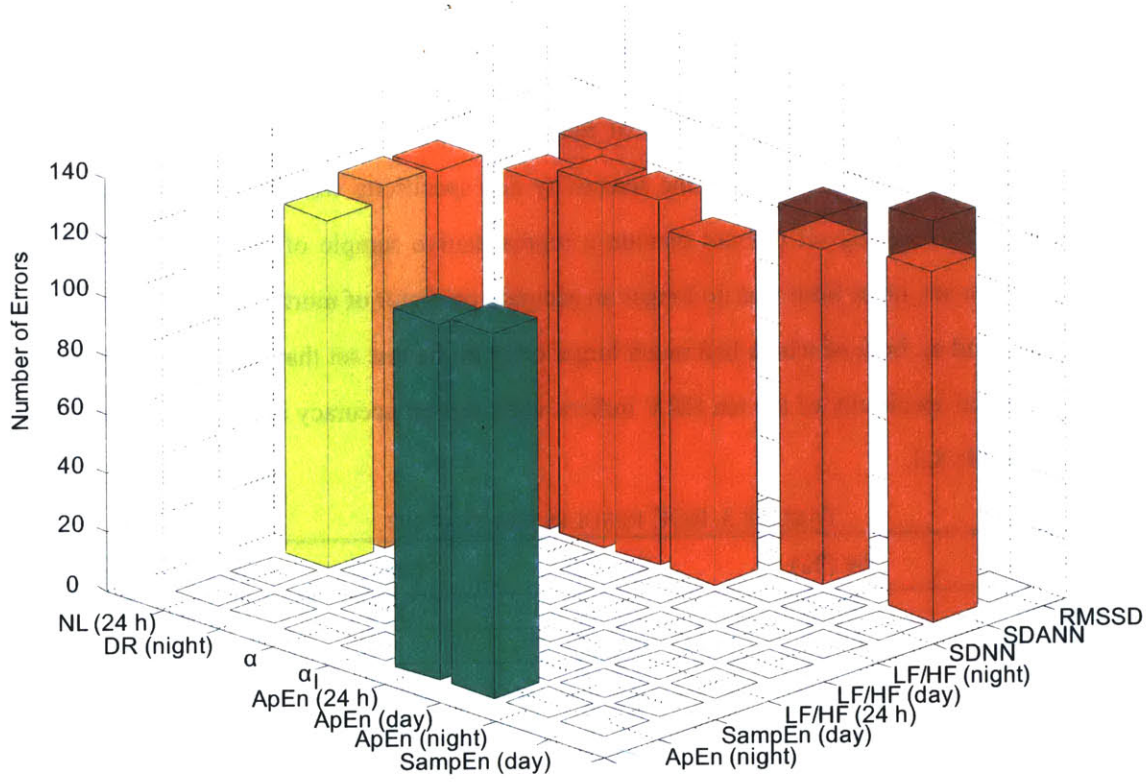

Figure 8.5. Support vector machine classification errors for test set (n = 358) from training set boundaries. Only the HRV index combinations that yielded a lower error than the best ROC detection (error = 125) are plotted.

TABLE 8.4. BEST 2-D SUPPORT VECTOR MACHINE CLASSIFIERS

HRV index 1	HRV index 2	Errors	Accuracy (%)
NL (24 h)	LF/HF (24 h)	101	71.63
NL (24 h)	LF/HF (day)	110	69.10
NL (24 h)	LF/HF (night)	112	68.54
DR (night)	SDNN	112	68.54
DR (night)	SDANN	112	68.54
α	SDNN	114	67.98
α_1	SDNN	115	67.70
ApEn (24 h)	ApEn (night)	117	67.13
ApEn (24 h)	SDNN	118	66.85
ApEn (24 h)	RMSSD	119	66.57

The boundaries for SVC of 5-year mortality based on NL (24 h) and LF/HF (24 h) are plotted in Figure 8.6, where the red marks indicate survivors and the blue marks indicate nonsurvivors. The left panel plots the training set data, where the circled data points are the support vectors. The right panel shows the test set data (asterisks) superimposed on the training set data (circles), where the classification errors are indicated by the red marks on the green background and the blue marks on the blue background.

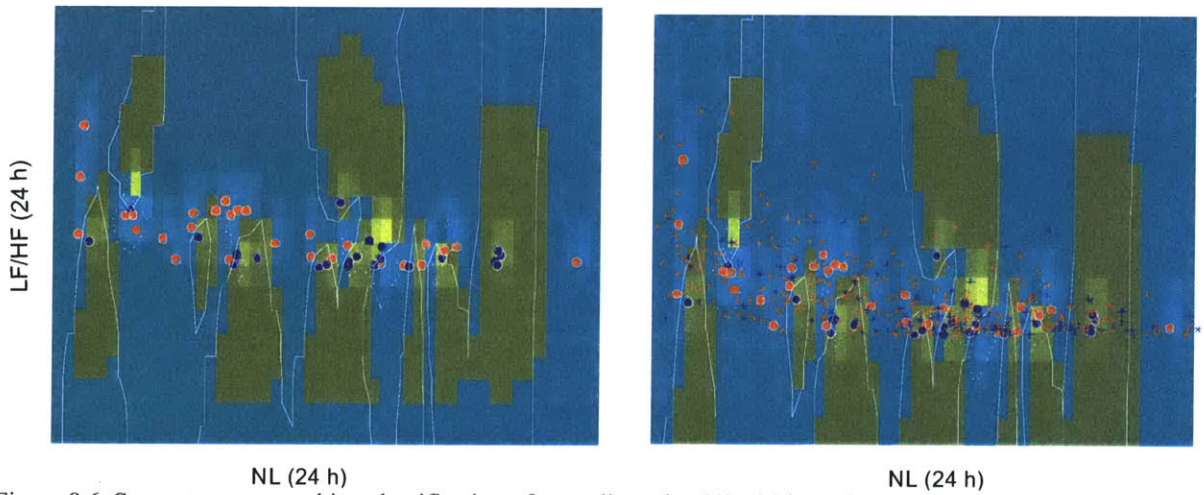

Figure 8.6. Support vector machine classification of mortality using NL (24 h) and LF/HF (24 h). The training set is plotted in the left panel and the test set is superimposed on the training set in the right panel for better observation of classification errors. The survivors are represented by the red marks and the nonsurvivors by the blue marks. The white lines indicate the support vectors.

In support vector machine classification combining three HRV indices, 77 different combinations yielded fewer than 125 errors. However, the minimum amount of errors for 3D analysis was 113, a number higher than the best two classifiers in the 2D SVC analysis. Thus, though the addition of a third parameter improved on many of the 2D classifiers, it had a detrimental effect on others. The six combinations of 3 HRV indices yielded 117 or fewer errors (11 combinations yielded 118 errors) are listed in Table 8.5.

TABLE 8.5. BEST3-D SUPPORT VECTOR MACHINE CLASSIFIERS

HRV index 1	HRV index 2	HRV index 3	Errors	Accuracy (%)
SampEn (night)	LF/HF (day)	RMSSD	113	68.26
α_l	LF/HF (day)	SDANN	114	67.98
NL (24 h)	$\alpha_{l,}$	LF/HF (24 h)	116	67.42
α_l	SampEn (24 h)	LF/HF (day)	116	67.42
α	α_s	LF/HF (day)	117	67.13
α	SampEn (night)	LF/HF (day)	117	67.13

Chapter 9 Complete Data Set Results

9.1 ROC Analysis of Complete Data Set

The ROC analysis results for the ten best detectors are shown in Table 9.1. The AUC values, sensitivity, and specificity were lower than those in the training set, as was expected from the decreased sensitivity and specificity of the test set (Section 8.2.1).Additionally, the critical values for the entire data set were slightly higher than those of the training set.

TABLE 9.1. INDICES WITH HIGHEST ACCURACY IN ROC ANALYSIS FOR COMPLETE DATA SET

Index	AUC	Se (%)	Sp (%)	Critical Value
LF/HF (day)	0.6768	60.85	73.23	1.45979
LF/HF (night)	0.6619	65.13	66.14	1.01717
LF/HF (24 h)	0.6726	66.90	63.78	1.08255
α_s	0.6716	59.08	70.08	0.80448
SDANN	0.6493	67.97	59.06	94.76 ms
SDNN	0.6490	67.62	59.06	105.63 ms
NL (24 h)	0.6297	64.57	60.14	55.26173
NL (day)	0.6233	62.21	61.57	55.45600
VLF (24 h)	0.6327	62.28	60.63	1110 ms^2
NL (night)	0.6289	73.23	52.31	50.58462

The five worst HRV detectors of mortality and their AUC for the entire data set (n=408) were: RMSSD (0.5256), pNN50 (0.5096), 24-hour SampEn (0.5746), day ApEn (0.5420), and night SampEn (0.5867). For ROC analysis on the entire data set, total power (TP) and high frequency (HF) were better detectors than for the training set, while entropy measures and α_1 were worse detectors.

9.2 Cox Proportional Hazards Model for All-Cause Death

The univariate Cox proportional hazards analysis for the complete data set (408 subjects) yielded the same number of significant variables as the training set analysis. The larger subject number resulted in much more significant (p value < 0.0000) univariate predictors. Twenty of the HRV indices were found to be significant univariate predictors of mortality (p value <0.05), where the VLF (day) was significant in the complete data set and not in the training set, whereas SampEn (day) and ApEn (day) were no longer

significant in the complete data set analysis. Table 9.2 shows the results for Cox univariate and multivariate analyses. The dashes in the multivariate columns indicate variables that were not entered in the model since they were not at least marginally significant in univariate prediction. HRV indices with a blank multivariate p value were eliminated from the multivariate model in the backwards selection of parameters. Multivariate analysis yielded surprisingly different results from those of the training set. The day LF/HF and were independent predictors of mortality, while the day and night DR were marginally significant in the multivariate model.

TABLE 9.2. RESULTS FOR COX PROPORTIONAL HAZARDS ANALYSIS OF THE COMPLETE DATA SET

Index	Log of Univariate Hazard Ratio	Univariate χ^2	Univariate P value	Multivariate P value
α_s	-0.6302	28.42	<0.0001	
LF/HF (day)	-0.1533	23.24	<0.0001	<0.0001
SDNN	-5.0010	22.84	<0.0001	0.0001
SDANN	-5.1369	22.37	<0.0001	
LF/HF (24 h)	-0.1556	21.67	<0.0001	
LF/HF (night)	-0.1403	17.94	<0.0001	
NL (24 h)	0.0075	15.89	<0.0001	
NL (day)	0.0076	15.28	<0.0001	
NL (night)	0.0065	14.63	0.0001	
SampEn (night)	-0.6046	12.25	0.0005	
DR (day)	0.5663	9.21	0.0024	
VLF (24 h)	-0.0002	9.11	0.0025	0.0952
DR (24 h)	0.5997	9.09	0.0026	
α_1	-0.5657	9.00	0.0027	
VLF (day)	-0.0002	8.89	0.0029	0.1121
ApEn (night)	-0.5830	8.27	0.0040	
SampEn (24 h)	-0.5120	7.16	0.0075	
DR (night)	0.4916	7.16	0.0075	
VLF (night)	-0.0001	6.60	0.0102	0.0730
ApEn (24 h)	-0.4636	4.37	0.0365	
LF (day)	-0.0002	2.48	0.1155	-
SampEn (day)	-0.2799	2.12	0.1457	-
TP (day)	-0.0000	2.03	0.1539	-
LF (24 h)	-0.0001	1.75	0.1861	-
TP (24 h)	-0.0000	1.59	0.2073	-
ApEn (day)	-0.2331	1.15	0.2830	-
LF (night)	-0.0001	0.79	0.3732	-
TP (night)	-0.0000	0.79	0.3745	-
pNN50	-0.5262	0.65	0.4199	-
RMSSD	0.5879	0.07	0.7983	-
HF (night)	0.0000	0.01	0.9168	-
HF (24 h)	0.0000	<0.00	0.9635	-
HF (day)	-0.0000	<0.00	0.9920	-

The difference in prediction between the best and worst mortality predictors is best represented by their Kaplan Meier survival curves. Such curves can be seen in Figure 9.1 for the three most significant univariate predictors in the left frame. The right frame of Figure 9.1 illustrates the Kaplan Meier curves for the 24-hour NL and night HF, in red and yellow respectively, both of which were significant univariate predictors of mortality (p value < 0.05), and the Kaplan Meier curves for night HF, a HRV index not significant in univariate prediction of mortality. The group characteristics (e.g. SDNN > 100 ms) are identified to the right of each curve.

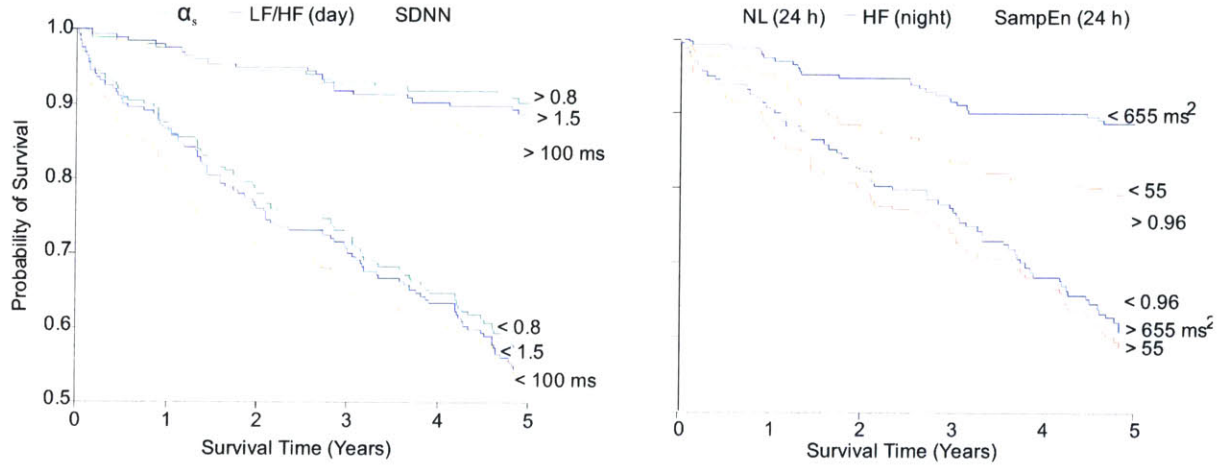

Figure 9.1. Kaplan Meier curves for entire data set. The left frame—short-term correlation exponent, LF/HF (day), and SDNN—plots the best mortality predictors. The right frame plots two worse, but significant, predictors (24 hour NL and SampEn) and a nonsignificant predictor (night HF).

The critical values for the division into high-risk and low-risk groups for the Kaplan Meier curves were those derived from ROC analysis of the entire data set. The goodness of the mortality predictors is clearly seen from the separation of the survival curves for groups above and below the critical values.

9.3 Cox Proportional Hazards Model for Sudden Death and Progressive Pump Failure

Survival analysis of the entire data set for prediction of sudden death yielded α_s and nighttime LF/HF to be significant (p value < 0.05) univariate predictors in the Cox proportional hazards model, whereas the LF/HF (day and 24 hour), day NL, and night VLF were marginally significant predictors of mortality (p

value < 0.10). Two additional absolute frequency indices, the LF and TP at night, were marginally significant univariate predictors of mortality, neither of which was a predictor for all-cause death. In the multivariate model beginning with all of the significant and marginally significant univariate predictors, only the night and 24-hour LF/HF and the night LF retained their significance after the backwards variable selection; such that these frequency indices are independent predictors of sudden death. The results for the Cox proportional hazards analysis of the significant and marginally significant univariate predictors of sudden death can be seen in Table 9.3.

TABLE 9.3. SIGNIFICANT UNIVARIATE PREDICTORS OF SUDDEN DEATH

Index	Log of Univariate Hazard Ratio	Univariate χ^2	Univariate P value	Multivariate P value
LF/HF (night)	-0.0964	4.11	0.0427	0.038
α_s	-0.3657	3.94	0.0471	
LF/HF (24 h)	-0.0837	3.52	0.0607	0.048
TP (night)	0.0000	3.28	0.0701	
LF (night)	0.0001	3.26	0.0708	0.036
NL (day)	0.0056	3.21	0.0732	
VLF (night)	0.0001	3.08	0.0793	
LF/HF (day)	-0.0662	2.76	0.0964	0.052

Analysis of predictors for death by progressive pump failure yielded results more similar to those of all-cause death than to those of sudden death. In addition to the significant univariate predictors for all-cause death, ApEn (day), LF (day), and SampEn (day) were also significant univariate predictors of death from progressive pump failure. A complete list of the significant univariate predictors of progressive pump failure death is shown in Table 9.4.

TABLE 9.4. SIGNIFICANT UNIVARIATE PREDICTORS OF PROGRESSIVE PUMP FAILURE DEATH

Index	Log of Univariate Hazard Ratio	Univariate χ^2	Univariate P value	Multivariate P value
α_s	-1.1093	31.63	<0.0000	0.0394
SDANN	-8.0386	23.19	<0.0000	0.0517
SDNN	-7.4949	22.37	<0.0000	
LF/HF (day)	-0.2952	21.10	<0.0000	
LF/HF (24 h)	-0.3049	20.12	<0.0000	0.0326
NL (night)	0.0108	17.40	<0.0000	0.0394
SampEn (night)	-1.0376	16.96	<0.0000	
LF/HF (night)	-0.2749	16.86	<0.0000	0.0429
NL (24 h)	0.0114	15.64	<0.0000	0.0429
ApEn (night)	-1.0921	14.22	0.0002	
SampEn (24 h)	-1.0177	13.13	0.0003	

NL (day)	0.0101	12.03	0.0005	
α_1	-0.9003	11.50	0.0007	
VLF (24 h)	-0.0003	10.48	0.0012	
VLF (night)	-0.0003	10.45	0.0012	
ApEn (24 h)	-1.0228	10.17	0.0014	
VLF (day)	-0.0003	7.52	0.0061	
SampEn (day)	-0.7515	6.58	0.0103	
DR (day)	0.7334	6.48	0.0109	
DR (24 h)	0.7842	6.42	0.0113	0.0429
DR (night)	0.6430	5.09	0.0241	
ApEn (day)	-0.6993	4.72	0.0299	
LF (day)	-0.0001	4.61	0.0317	

In the backwards selection multivariate model, the short-range exponent, 24-hour and night LF/HF, 24-hour DR, and 24-hour and night noise limit were significant while the SDANN was marginally significant predictors of progressive pump failure death. Thus, more HRV indices are independent predictors of progressive pump failure than of sudden death or all-cause death. Kaplan-Meier survival curves for several significant univariate predictors of sudden death and progressive pump failure are plotted in Figure 9.2.

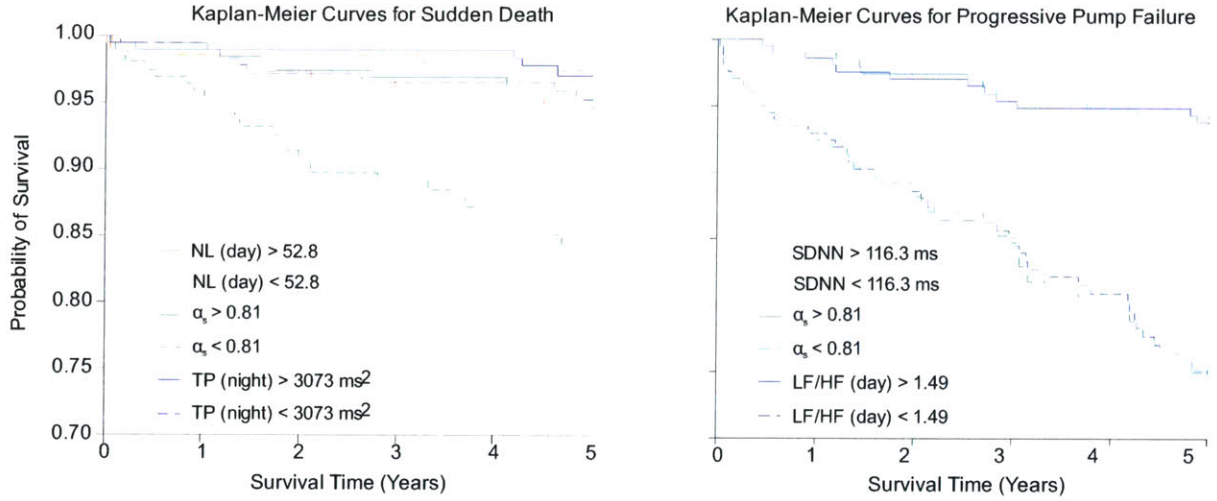

Figure 9.2. Kaplan-Meier curves for sudden death and progressive pump failure. The left panel plots the survival curves for the day NL, short-range correlation exponent, and night TP in sudden death. The right panel plots the survival curves for SDNN, short-range correlation exponent, and day LF/HF in progressive pump failure. The cut-off values were determined by the median HRV indices in the entire population.

Chapter 10 Discussion of Results and Significance of Study

10.1 Analysis and Interpretation of Results

The results described in Chapters 8 and 9 provide insight into the different HRV indices that indicate a high risk of death in CHF subjects and, more importantly, which indices describe a particular kind of death. These findings are of key importance in providing physicians with an additional non-invasive tool for determining the optimal treatment for the patient. The results presented in Chapter 9 shows LF/HF to be an independent predictor of all-cause death, sudden death, and progressive pump failure death, whereas other HRV indices such as LF, SDANN, the short-range exponent, and NL are independent predictors of a particular kind of death. Further analysis of the physiological significance of the indices and the differences between the survivor and non-survivor groups leads to better characterization of the mortality predictors and the physiological indicators of sudden death or pump failure death.

Receiver operating characteristic analysis with the training set and test set did not yield satisfactory results due to the special characteristics of the training set. The training set had been chosen randomly by a third party, however, as is apparent from the decreased accuracy of the test set, the HRV indices of the training set were not representative of those of the entire population. In addition, the percentage of deaths in both groups was greatly difference, with 54% survivors in the training set (n=50) and 69% survivors in the entire data set (n=408). Though the NL yielded the highest accuracy in distinguishing the survivors and nonsurvivors in the training set, the LF/HF index yielded the highest accuracy for ROC analysis in the test set. These results suggest the LF/HF is more consistently decreased in the nonsurvivors whereas the noise limit varies more in individual patients and was thus not accurately represented in the training set. In addition, the larger decrease in accuracy in the noise limit than in the LF/HF for the test set is explained by the AUC of both indices, where the AUC of LF/HF in the training set was higher representing a better test for survival. The support vector machine classification (SVC) yielded more accurate results than the ROC analysis, yet due to the faulty training set, the accuracy was not optimal. However, the combinations of HRV indices that resulted in the more accurate mortality detections suggest indices that complement each other. If two HRV indices provided contradictory information,

accuracy would be severely compromised. Thus, from SVC analysis we conclude that a combination of the NL and LF/HF would result in the most accurate 2-dimensional 5-year mortality detector. SVC analysis also suggests traditional time-domain measures agree with nonlinear and complexity analyses such that the accuracy of SDNN, SDANN, and RMSSD—measures of overall HRV, low-frequency oscillations, and high-frequency oscillations respectively—can be increased by a combination with nonlinearity detection rate, DFA indices, or entropy measures. Though the physiological interpretations of the nonlinear and complexity measures are not as well established as those of the time-domain indices, this study shows they do not present contradictory information and can potentially be used together to yield a better prediction of mortality in CHF.

ROC analysis provides information on which indices are best at distinguishing 5-year mortality without accounting for the time of death. The outputs of ROC analysis, the sensitivity and specificity allow for the critical value to be chosen so as to minimize the errors with the largest cost, while limiting those errors to be the output of a simple threshold test. The limitation of ROC analysis to one variable at a time with a set linear threshold motivated the need for support vector machine classification. SVC should produce the same results as ROC for a single variable classification and a linear kernel. The 2- and 3-dimensional SVC with the Gaussian RBF kernel improve on the linear 1-dimensional detector; however, the complexity is greatly increased for testing of the HRV indices. Thus, the SVC results must be taken as a preliminary test for which combinations of HRV indices would be most accurate in identifying 5-year mortality in the CHF patients. The Cox proportional hazards model presents the results with most value to the study, where a training set was not necessary for analysis, and the risk function is calculated as a summation in log space rather than linear space. Though survival analysis produces a data point every time an event occurs, the hazard ratio is constant in time, such that the significance of a variable in predicting mortality is independent of the time of death of each patient. In addition, the Cox model allows for a weighted combination of HRV indices in order to determine which indices are independent predictors of death when others are present. The survival curves in the analysis judge the risk of death of a patient with a high or low HRV index at any point in time. The results for survival analysis in the training also differ from those of the entire database, such that only the results for the database will be discussed.

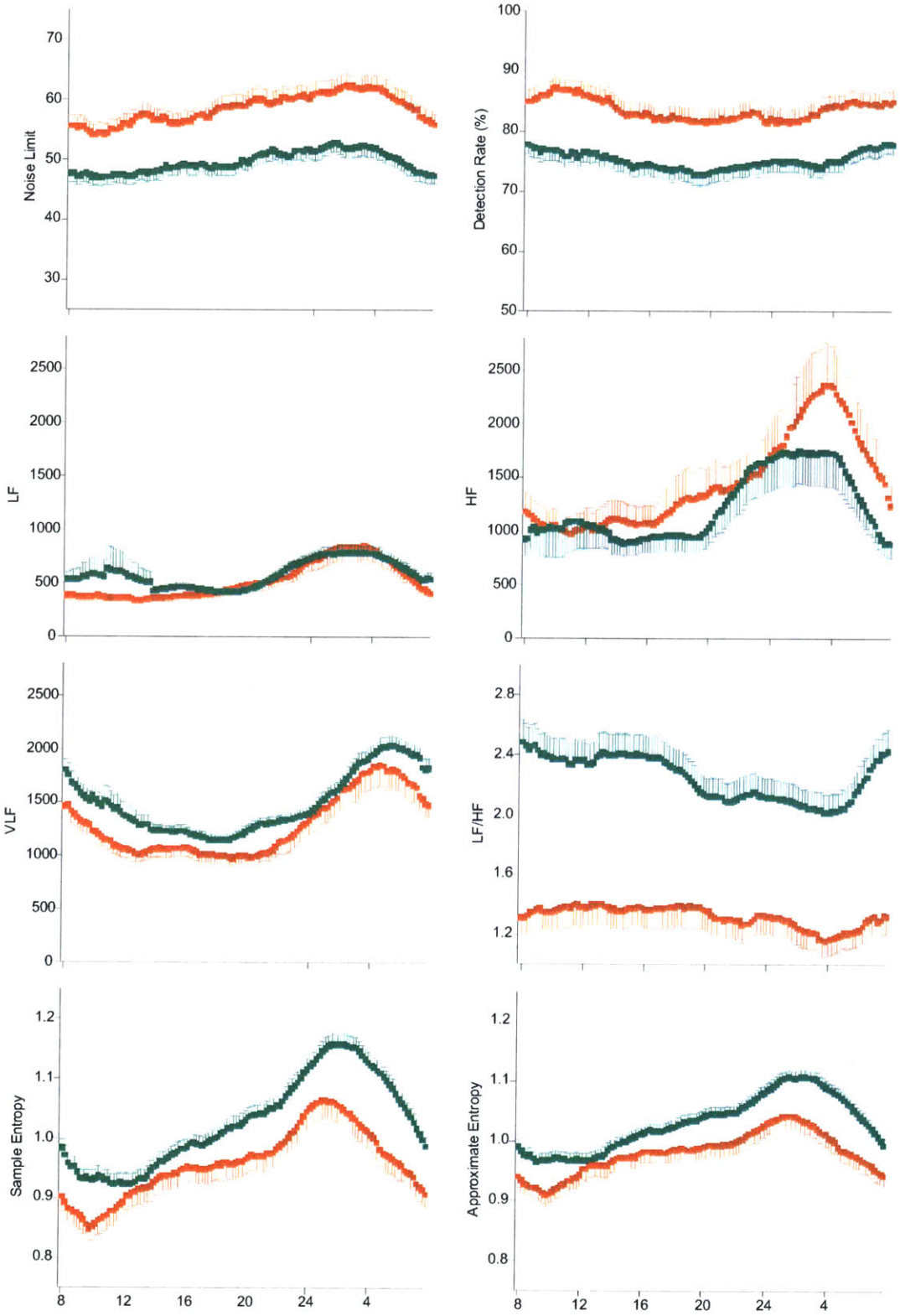

Figure 10.1. Group averages for HRV indices. The mean (SE) noise limit, detection rate, low frequency, high frequency, very low frequency, LF/HF, sample entropy, and approximate entropy of 12-minute segments in a 24-hour period are plotted for the survivor and nonsurvivor group.

The results of ROC analysis and survival analysis for the entire dataset can be understood from the plots in Figures 10.1 and 10.2. Figure 10.1 plots several of the HRV indices which were analyzed according to the time (day, night, 24-hour) and illustrates the importance of the time divisions by means of the circadian rhythms. Figure 10.2 shows the variables which were only measured in the 24-hour period.

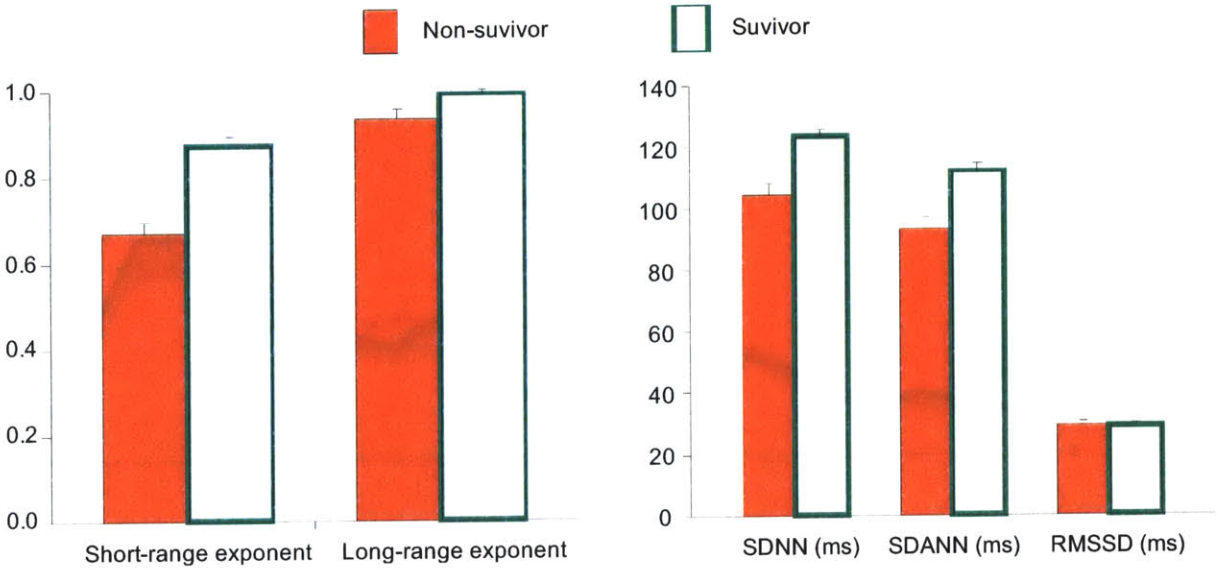

Figure 10.2. Mean and standard-error for 24-hour variables. The left panel shows the DFA exponents and the right panel shows some time-domain indices.

The lack of all-cause mortality prediction power of the low- and high-frequency components is apparent from Figure 10.1, where the survivor and non-survivor groups have overlapping mean values throughout the 24-hours. However, the slightly higher value of HF for the nonsurvivor group and the slightly higher value of LF for the survivor group contribute to the wide separation of the two groups in the LF/HF. The figure also shows chaos analysis yields a significant difference in both the noise limit and the nonlinearity detection rate between the survivors and nonsurvivors. Similar to the high-frequency component, the chaos indices were higher in the nonsurvivor group, however, neither group had an apparent circadian rhythm for the chaos indices. The circadian rhythm of the HRV indices has the largest effect on the group distinction with the entropy measures and the very-low frequency component. These plots illustrate the necessity for the index to be evaluated during the day, night, and 24-hour to maximize group distinction. In Figure 10.2, the mean (SE) values for 24-hour HRV indices are plotted, where the nonsurvivor values are represented by the red bars and the survivor values by the blank bars with green outline. The large significance of the short-range exponent, SDNN, and SDANN as univariate predictors can be understood

from Figure 10.2. The average value of the RMSSD is similar for the survivors and nonsurvivors, explaining the lack of prediction power for this parameter.

The results for survival analysis agreed with many of those in the literature, however, this is the first time that independent predictors of mortality are chosen from such a wide variety of HRV indices. As in various previous studies, SDNN was found to be a univariate predictor of all-cause mortality [10, 45, 67, 75, 78] as well as a significant predictor of death in the multivariate model. Similar to other studies, the VLF and LF/HF also resulted to be significant univariate predictors of mortality as well as independent predictors in the multivariate model [10, 77, 78] while the LF and HF components were not significant risk factors of all-cause mortality [77, 78]. However, though the short-range exponent was a significant univariate predictor of all-cause death as in Makikallio's study [78], it was not an independent predictor of mortality in the multivariate model. This could be explained by the inclusion of the LF/HF term in multivariate analysis which is also a measure of sympathovagal balance. Inclusion of the chaos parameters, NL and DR, in the univariate analysis yielded both NL and DR to be significant univariate predictors but not independent predictors of all-cause mortality. Though the relationship between chaos and physiology is not well understood, it has been proposed that the level of chaos in the heart rate is a combination of intrinsic chaos and a larger component of respiratory chaos affecting the heart through the vagal input [97]. Sympathetic mechanisms do not participate in the respiratory arrhythmia [98], from which respiratory chaos arises. In addition, a correlation has been established between the LF/HF and the noise limit; the noise limit, a relative measure of chaos intensity, is increased with a larger chaotic component (HF) in CHF subjects whereas a larger non-chaotic component (LF) acts as a noise-floor and decreases the detected chaos level [97]. Though the survival analysis for all-cause death determined HRV indices which indicate a high risk of death, predictors of specific kinds of death provide more insight into risk stratification for fatal physiological events and thus aid in the treatment of the disease.

Cox univariate analysis for sudden death yielded fewer significant predictors than that of all-cause death,. The difference is likely due to the smaller population which suffered an event (n=48 for sudden death and n=127 for all-cause death) and the different mechanisms of death that were combined for the all-cause death analysis. As in previous studies, the night LF component, which was not a significant predictor of all-cause death, was a significant univariate and multivariate predictor of sudden death [73, 80, 81]. The

LF/HF was found to be both a univariate predictor, as in [81], and a multivariate predictor of sudden death. Since this HRV index was also an independent predictor for all-cause death and progressive pump failure death, and the LF/HF value is decreased for all kinds of deaths, the index can be utilized as a predictor for 5-year mortality without detailing what physiological mechanism might cause death or what medications might be most beneficial for the patient. The night LF component, however, is particular to sudden death since it is not a univariate predictor for all-cause death or progressive pump failure death.

Survival analysis for progressive pump failure yielded the short-range exponent, LF/HF (24-hour and nighttime), and NL (24-hour and nighttime) to be independent predictors of pump failure death whereas the SDANN index was marginally significant in the multivariate model. With the exception of the LF/HF, the significance of the other HRV indices is limited to the prediction of death from progressive pump failure. Risk stratification for progressive pump failure death has not been as widely studied as that for sudden death, and the results of the current study provide additional insight for the characterization of progressive pump failure. Kearney previously found SDNN (SDANN was not tested) to be an independent predictor of progressive pump failure [71], however, in the presence of SDANN, frequency, chaos, and entropy indices, SDANN retained marginal significance in the multivariate model while SDNN was significant only in the univariate model. Contrary to previous studies [45, 80], none of the absolute frequency indices were independent predictors of progressive pump failure death. To our knowledge, DFA parameters have never been tested as predictors for specific kinds of death in heart failure. This study shows a decreased short-range exponent to be an independent predictor of death from progressive pump failure. This can be interpreted as autonomic imbalance [48], where those who died from progressive heart failure experienced less reciprocal changes in the sympathetic and vagal activity as is characteristic of CHF. The final major contribution of this study to the analysis of death from progressive heart failure is the risk stratification power of the noise limit. A decrease in the chaoticity of the heart rate had been previously reported for CHF patients [66] in the more severe stages of the disease. However, the difference in chaos level of the heart rate has not been studied within the CHF population. In this study we found increased noise limit, both for the nighttime and the 24-hour period, to be an independent predictor of death from progressive pump failure. Though an accurate physiological interpretation merits further study, this result suggests the chaoticity of the heart rate of patients at risk for progressive pump failure death assimilates that of healthy subjects than that of severe CHF patients.

This study, for the first time, analyzed the predictors of all-cause mortality, sudden death, and death from progressive heart failure with a comprehensive set of heart rate variability indices. The LF/HF (day), SDNN, and VLF (24-hour and night) indices were independent predictors of all-cause death, whereas the LF/HF (24-hour and night) and LF (night) were independent predictors of sudden death and the short-range exponent, LF/HF (24-hour and night), and NL (24-hour and night) were independent predictors of death from progressive heart failure. Thus, LF/HF presents the best marker for 5-year mortality in CHF patients. As has been previously reported, the nighttime low-frequency component provides insight into the risk of sudden death whereas novel results indicate the short-range exponent and the noise limit are selective for progressive pump failure death. All of the predictive indices suggest a high risk of death in CHF can be identified by the autonomic imbalance that accompanies the disease and thus present an additional tool for physicians to determine the best course of treatment to reduce the risk of death.

10.2 Study Limitations and Future Work

Results of the current study might not correspond to those of previous studies due to experimental design differences such as population sizes, percentage of deaths, and follow-up period. The significance of the variables in the current analysis is contingent on independent prediction power from physiological parameters. As other studies have found significant univariate predictors to not be independent predictors of mortality in the presence of chemical factors and physiological measurements, the current analysis would be improved by including other factors such as age, sodium, creatinine, and left ventricular ejection fraction in the multivariate model determination. Further analysis of the patient characteristics for the high-risk and low-risk groups for types of death could also lead to a more in depth understanding of the mechanisms of sudden death and progressive pump failure in relation to heart rate variability. Classification of patient characteristics with high and low short-range exponent or noise limit could also lead to a more comprehensive physiological interpretation of these HRV indices for which the physiological characteristics have not been well-studied.

Alternate extensions of the current study involve an expansion of the patient population. The addition of age-matched healthy subjects would aid in the physiological interpretation of the less-known HRV

indices such as the short-range exponent and the noise limit. Alternate analyses could include different groups of the CHF population such as patients treated with more modern techniques (e.g. beta-blockers) or patients with more advanced stages of the disease. However, these analyses share the goal of disease and heart rate variability index characterization rather than survival analysis in congestive heart failure.

References

[1] M. W. Derstine, H. M. Gibbs, F. A. Hopf, and L. D. Sanders, "Distinguishing chaos from noise in an optically bistable system," *IEEE Journal of Quantum Electronics,* vol. QE-21, pp. 1419-1422, 1985.

[2] J. B. Gao, J. Hu, W. W. Tung, and Y. H. Cao, "Distinguishing chaos from noise by scale-dependent Lyapunov exponent," *Physical Review E,* vol. 74, p. 066204, 2006.

[3] C.-S. Poon and M. Barahona, "Titration of chaos with added noise," *PNAS,* vol. 98, pp. 7107-7112, June 19, 2001 2001.

[4] J. B. Gao, C. C. Chen, S. K. Hwang, and J. M. Liu, "Noise-induced chaos," *International Journal of Modern Physics B,* vol. 13, pp. 3283-3305, 1999.

[5] J. B. Gao, S. K. Hwang, and J. M. Liu, "Effects of intrinsic spontaneous-emission noise on the nonlinear dynamics of an optically injected semiconductor laser," *Physical Review A,* vol. 59, pp. 1582-1585, 1999.

[6] F. Gassmann, "Noise-induced chaos-order transitions" *Physical Review E,* vol. 55, pp. 2215-2221, 1997.

[7] M. Strumik, W. M. Macek, and S. Redaelli, "Discriminating additive from dynamical noise for chaotic time series," *Physical Review E,* vol. 72, p. 0363219, 2005.

[8] S. Goldman, G. Johnson, J. N. Cohn, G. Cintron, R. Smith, and G. Francis, "Mechanism of death in heart failure. The Vasodilator-Heart Failure Trials.," *Circulation,* vol. 87, pp. VI24-31, 1993.

[9] M. O. Sweeney, "Sudden death in heart failure assicuated with reduced left ventricular function: substrates, mechanisms, and evidence-based management, part I," *Pacing and Clinical Electrophysiology,* vol. 24, pp. 871-888, 2001.

[10] G. R. H. Sandercock and D. A. Brodie, "The Role of Heart Rate Variability in Prognosis for Different Modes of Death in Chronic Heart Failure," *Pacing Clin Electrophysiol,* vol. 29, pp. 892-904, 2006.

[11] R. Gilmore and M. Lefranc, *The Topology of Chaos*. New York: John Wiley & Sons, Inc, 2002.

[12] S. H. Strogatz, *Nonlinear Dynamics and Chaos*. Cambridge: Perseus 1994.

[13] V. S. Anishchenko, V. V. Astakhov, A. B. Neiman, T. E. Vadivasova, and L. Schimansky-Geier, *Nonlinear Dynamics of Chaotic and Stochastic Systems: Tutorial and Modern Developments*. Berlin: Springer, 2002.

[14] B. Dennis, R. A. Desharnais, J. M. Cushing, S. M. Henson, and R. F. Costantino, "Can noise induce chaos?," *Oikos,* vol. 102, pp. 329-339, 2003.

[15] A. Zaikin and J. Kurths, "Additive noise in noise-induced nonequilibrium transitions," *Chaos,* vol. 11, pp. 570-580, 2001.

[16] A. L. Goldberger and B. J. West, "Chaos in physiology: health or disease?," in *Chaos in Biological Systems*, H. Degn, A. V. Holden, and L. F. Olsen, Eds. New York: Plenum Press, 1987.

[17] J. B. Bassingthwaighte, *Fractal physiology*. New York: Oxford University Press, 1994.

[18] J. E. Skinner, "Low-dimensional chaos in biological systems," *Biotechnology,* vol. 12, pp. 596-600, 1994.

[19] J. N. Weiss, A. Garfinkel, M. L. Spano, and W. L. Ditto, "Chaos and chaos control in biology," *J Clin Invest,* vol. 93, pp. 1355-1360, 1994.

[20] B. J. West, *Fractal physiology and chaos in medicine* vol. 1, 1990.

[21] A. Babloyantz and A. Destexhe, "Low-dimensional chaos in an instance of epilepsy," *Proc Natl Acad Sci USA,* vol. 83, pp. 3513-3517, 1986.

[22] C. C. Canavier, J. W. Clark, and J. H. Byrne, "Routes to chaos in a model of a bursting neuron," *Biophys J,* vol. 57, pp. 1245-1251, 1990.

[23] S. Sinha and R. Ramaswamy, "Dynamics of controlled metabolic network and cellular behaviour," in *Chaos in Biological Systems*, H. Degn, A. V. Holden, and L. F. Olsen, Eds. New York: Plenum Press, 1987.

[24] M. Hénon, "A Two-dimensional Mapping with a Strange Attractor," *Comm Math Phys,* vol. 50, pp. 69-77, 1976.

[25] K. Ikeda, "Multiple-valued stationary state and its instability of the transmitted light by a ring cavity system," *Optics Communications,* vol. 30, pp. 257-261, 1979.

[26] Z. Galias, "Rigorous investigation of the Ikeda map by means of interval arithmetic," *Nonlinearity,* vol. 15, pp. 1759-1779, 2002.

[27] E. N. Lorenz, "Deterministic Nonperiodic Flow," *Journal of the Atmospheric Sciences,* vol. 20, pp. 130-141, 1963.

[28] H. Azhar, K. Iftekharuddin, and R. Kozma, "A Chaos Synchronization-Based Dynamic Vision Model for Image Segmentation," in *International Joint Conference on Neural Networks*, Montreal, 2005.

[29] M. C. Mackey and L. Glass, "Oscillation and Chaos in Physiological Control Systems," *Science,* vol. 197, pp. 287-289, 1977.

[30] B. Mensour and A. Longtin, "Power spectra and dynamical invariants for delay-differential and difference equations," *Physica D,* vol. 113, pp. 1-25, 1998.

[31] M. Barahona and C.-S. Poon, "Detection of nonlinear dynamics in short, noisy time series," *Nature,* vol. 381, pp. 215-217, 1996.

[32] M. J. Korenberg, "Orthogonal identification of nonlinear difference equation models," in *Proc. 28th Midwest Symp. Circuit Sys.*, 1985, pp. 90-95.

[33] C. Letellier and E. M. Mendes, "Robust discretizations versus increase of the time step for the Lorenz system," *Chaos,* vol. 15, p. 13110, 2005.

[34] M. J. Korenberg, "Identifying nonlinear difference equation and functional expansion represenations: the fast orthogonal algorithm," *Annals of Biomedical Engineering,* vol. 16, pp. 123-142, 1988.

[35] K. H. Chon, M. J. Korenberg, and N. H. Holstein-Rathlou, "Application of fast orthogonal search to linear and nonlinear stochastic systems," *Annals of Biomedical Engineering,* vol. 25, pp. 793-801, 1997.

[36] G. W. Moe and P. W. Armstrong, "Congestive heart failure," *CMAJ,* vol. 138, pp. 689-694, 1988.

[37] E. K. Massin, "Outpatient management of congestive heart failure," *Tex Heart Inst J,* vol. 25, pp. 238-250, 1998.

[38] J. S. Floras, "Sympathetic activation in human heart failure: diverse mechanisms, therapeutic opportunities," *Acta Physiol Scand,* vol. 177, pp. 391-398, 2003.

[39] G. Grassi, G. Seravalle, B. M. Cattaneo, A. Lanfranchi, S. Vailati, C. Giannattasio, A. D. Bo, C. Sala, G. B. Bolla, M. Pozzi, and G. Mancia, "Sympathetic activation and loss of reflex sympathetic control in mild congestive heart failure," *Circulation,* vol. 92, pp. 3206-3211, 1995.

[40] T. R. Porter, D. L. Eckberg, J. M. Fritsch, R. F. Rea, L. A. Beightol, J. F. Schmedtje, and P. Mohanty, "Autonomic Pathophysiology in Heart Failure Patients," *J Clin Invest,* vol. 85, pp. 1362-1371, 1990.

[41] M. Rubart and D. P. Zipes, "Mechanisms of sudden cardiac death," *J Clin Invest,* vol. 115, pp. 2305-2315, 2005.

[42] R. Freeman, "Assessment of cardiovascular autonomic function," *Clinical Neurophysiology,* vol. 117, pp. 716-730, 2006.

[43] M. T. Kearney, J. Nolan, A. J. Lee, P. W. Brooksby, R. Prescott, A. M. Shah, A. G. Zaman, D. L. Eckberg, H. S. Lindsay, P. D. Batin, R. Andrews, and K. A. A. Fox, "A prognostic index to predict long-term mortality in patients with mild to moderate chronic heart failure stabilised on angiotensin converting enzyme inhibitors," *European Journal of Heart Failure,* vol. 5, pp. 489-497, 2003.

[44] Task Force of the European Society of Cardiology and the North American Society of Pacing and Electrophysiology, "Heart Rate Variability : Standards of Measurement, Physiological Interpretation, and Clinical Use," *Circulation,* vol. 93, pp. 1043-1065, March 1, 1996 1996.

[45] B. M. Szabo, D. J. v. Veldhuisen, N. v. d. Veer, J. Brouwer, P. A. D. Graeff, and H. J. G. Crijns, "Prognostic Value of Heart Rate Variability in Chronic Congestive Heart Failure Secondary to Idiopathic or Ischemic Dilated Cardiomyopathy," *Am J Cardiol,* vol. 79, pp. 978-980, 1997.

[46] A. J. E. Seely and P. T. Macklem, "Complex systems and the technology of variability analysis," *Critical Care,* vol. 8, pp. R367-R384, 2004.

[47] A. Malliani, M. Pagani, F. Lombardi, and S. Cerutti, "Cardiovascular neural regulation explored in the frequency domain," *Circulation,* vol. 84, pp. 482-492, 1991.

[48] M. P. Tulppo, A. M. Kiviniemi, A. H. Hautala, M. Kallio, T. Seppanen, T. H. Makikallio, and H. V. Huikuri, "Physiological Background of the Loss of Fractal Heart Rate Dynamics," *Circulation,* vol. 112, pp. 314-319, 2005.

[49] J. J. Zebrowski and R. Baranowski, "Nonlinear Instabilities and Nonstationarity in Human Heart-Rate Variability," *Computing in Science & Engineering,* vol. 6, pp. 78-83, 2004.

[50] G. Jackson, C. R. Gibbs, M. K. Davies, and G. Y. H. Lip, "ABC of heart failure: Pathophysiology," *BMJ,* vol. 320, pp. 167-170, 2000.

[51] W. N. Leimbach, B. G. Wallin, R. G. Victor, P. E. Aylward, G. Sundlof, and A. L. Mark, "Direct evidence from intraneural recordings for increased central sympathetic outflow in patients with heart failure," *Circulation,* vol. 73, pp. 913-919, 1986.

[52] A. L. Goldberger, V. Bhargava, B. J. West, and A. J. Mandell, "On a mechanism of cardiac electrical stability. The fractal hypothesis.," *Biophys J,* vol. 48, pp. 525-528, 1985.

[53] F. Lombardi, "Chaos Theory, Heart Rate Variability, and Arrhythmic Mortality," *Circulation,* vol. 101, pp. 8-10, 2000.

[54] P. C. Ivanov, L. A. Nunes Amaral, A. L. Goldberger, S. Havlin, M. G. Rosenblum, Z. R. Struzik, and H. E. Stanley, "Multifractality in human heartbeat dynamics," *Nature,* vol. 399, pp. 461-465, 1999.

[55] R. W. Glenny, T. Robertson, S. Yamashiro, and J. B. Bassingthwaighte, "Applications of fractal analysis to physiology," *J Appl Physiol,* vol. 70, pp. 2351-2367, 1991.

[56] D. T. Kaplan, M. I. Furman, S. M. Pincus, S. M. Ryan, L. A. Lipsitz, and A. L. Goldberger, "Aging and the complexity of cardiovascular dynamics," *Biophys J,* vol. 59, pp. 945-949, 1991.

[57] D. C. Shannon, D. W. Carley, and H. Benson, "Aging of modulation of heart rate," *Am J Physiol Heart Circ Physiol,* vol. 253, pp. H874-H877, 1987.

[58] F. Beckers, B. Verheyden, and A. E. Aubert, "Aging and nonlinear heart rate control in a healthy population," *Am J Physiol Heart Circ Physiol,* vol. 290, pp. H2560-H2570, 2006.

[59] Z.-D. Deng, C.-S. Poon, N. M. Arzeno, and E. S. Katz, "Heart rate variability in pediatric obstructive sleep apnea," in *Conference Proceedings. Annual International Conference of the IEEE Engineering in Medicine and Biology Society*, New York, NY, USA, 2006.

[60] L. Zapanta, C.-S. Poon, D. P. White, C. L. Marcus, and E. S. Katz, "Heart Rate Chaos in Obstructive Sleep Apnea in Children," in *IEEE Trans Eng Med Biol.* vol. 6, 2004, pp. 3889-3892.

[61] J. P. Saul, Y. Arai, R. D. Berger, L. S. Lilly, W. S. Colucci, and R. J. Cohen, "Assessment of Autonomic Regulation in Chronic Congestive Heart Failure by Heart Rate Spectral Analysis," *Am J Cardiol,* vol. 61, pp. 1292-1299, 1988.

[62] S. Guzzetti, S. Mezzetti, R. Magatelli, A. Porta, G. D. Angelis, G. Rovelli, and A. Malliani, "Linear and non-linear 24 h heart rate variability in chronic heart failure," *Auton Neurosci,* vol. 86, pp. 114-119, 2000.

[63] S. G. Kim and M. K. Yum, "Decreased RR Interval Complexity and Loss of Circadian Rhythm in Patients With Congestive Heart Failure," *Jpn Circ J,* vol. 64, pp. 39-45, 2000.

[64] M. G. Signorini, S. Guzzetti, C. Manzoni, S. Milani, and S. Cerutti, "Multiparametric analysis of HRV signal by linear and nonlinear methods in heart failure patient population," 1998, pp. 322-325 vol.1.

[65] F. Lombardi and A. Mortara, "Heart rate variability and cardiac failure," *Heart,* vol. 80, pp. 213-214, September 1, 1998 1998.

[66] C.-S. Poon and C. K. Merrill, "Decrease of cardiac chaos in congestive heart failure," *Nature,* vol. 389, pp. 492-495, 1997.

[67] J. Nolan, P. D. Batin, R. Andrews, S. J. Lindsay, P. Brooksby, M. Mullen, W. Baig, A. D. Flapan, A. Cowley, R. J. Prescott, J. M. M. Neilson, and K. A. A. Fox, "Prospective Study of Heart Rate Variability and Mortality in Chronic Heart Failure : Results of the United Kingdom Heart Failure Evaluation and Assessment of Risk Trial (UK-Heart)," *Circulation,* vol. 98, pp. 1510-1516, October 13, 1998 1998.

[68] M. T. Kearney, A. Zaman, D. L. Eckberg, A. J. Lee, K. A. A. Fox, A. M. Shah, R. J. Prescott, W. E. Shell, E. Charuvastra, T. S. Callahan, W. P. Brooksby, D. J. Wright, N. P. Gall, and J. Nolan, "Cardiac size, autonomic function, and 5-year follow-up of chronic heart failure patients with severe prolongation of ventricular activation," *Journal of Cardiac Failure,* vol. 9, pp. 93-99, 2003.

[69] P. A. MacCarthy, M. T. Kearney, J. Nolan, A. J. Lee, R. J. Prescott, A. M. Shah, W. P. Brooksby, and K. A. A. Fox, "Prognosis in heart failure with preserved left ventricular systolic function: prospective cohort study," *BMJ,* vol. 327, pp. 78-79, July 10, 2003 2003.

[70] M. T. Kearney, K. A. A. Fox, A. J. Lee, W. P. Brooksby, A. M. Shah, A. Flapan, R. J. Prescott, R. Andrews, P. D. Batin, D. L. Eckberg, N. Gall, A. G. Zaman, H. S. Lindsay, and J. Nolan, "Predicting sudden death in patients with mild to moderate chronic heart failure," *Heart,* vol. 90, pp. 1137-1143, October 1, 2004 2004.

[71] M. T. Kearney, K. A. Fox, A. J. Lee, R. J. Prescott, A. M. Shah, P. D. Batin, W. Baig, S. Lindsay, T. S. Callahan, W. E. Shell, D. L. Eckberg, A. G. Zaman, S. Williams, J. M. Neilson, and J. Nolan, "Predicting death due to progressive heart failure in patients with mild-to-moderate chronic heart failure," *J Am Coll Cardiol,* vol. 40, pp. 1801-1808, 2002.

[72] N. Chattipakorn, T. Incharoen, N. Kanlop, and S. Chattipakorn, "Heart rate variability in myocardial infarction and heart failure," *Int J Cardiol,* 2007.

[73] M. Galinier, A. Pathak, J. Fourcade, C. Androdias, D. Curnier, S. Varnous, S. Boveda, P. Massabuau, M. Fauvel, J. M. Senard, and J. P. Bounhoure, "Depressed low frequency power of heart rate variability as an independent predictor of sudden death in chronic heart failure," *Eur Heart J,* vol. 21, pp. 475-482, 2000.

[74] W. Jiang, W. R. Hathaway, S. McNulty, and R. L. Larsen, "Ability of Heart Rate Variability to Predict Prognosis in Patients With Advanced Congestive Heart Failure," *The American Journal of Cardiology,* vol. 80, pp. 808-811, 1997.

[75] P. Ponikowski, S. D. Anker, T. P. Chua, R. Szelemei, M. Piepoli, S. Adamopoulos, K. Webb-Peploe, D. Harrington, W. Banasiak, K. Wrabec, and A. J. S. Coats, "Depressed Heart Rate Variability as an Independent Predictor of Death in Chronic Congestive Heart Failure Secondary to Ischemic or Idiopathic Dilated Cardiomyopathy," *Am J Cardiol,* vol. 79, pp. 1645-1650, 1997.

[76] K. K. L. Ho, G. B. Moody, C.-K. Peng, J. E. Mietus, M. G. Larson, D. Levy, and A. L. Goldberger, "Predicting Survival in Heart Failure Case and Control Subjects by Use of Fully Automated Methods for Deriving Nonlinear and Conventional Indices of Heart Rate Dynamics," *Circulation,* vol. 96, pp. 842-848, 1997.

[77] J. Brouwer, D. J. V. Veldhuisen, A. J. Man, J. Haaksma, A. Dijk, K. R. Visser, F. Boomsma, P. H. J. M. Dunselman, and K. I. Lie, "Prognostic Value of Heart Rate Variability During Long-Term Follow-Up in Patients With Mild to Moderate Heart Failure," *JACC,* vol. 28, pp. 1183-1189, 1996.

[78] T. H. Makikallio, H. Huikuri, U. Hintze, J. Videbaek, R. D. Mitrani, A. Castellanos, R. J. Myerburg, and M. Moller, "Fractal Analysis and Time- and Frequency-Domain Measures of Heart Rate Variability as Predictors of Mortality in Patients With Heart Failure," *Am J Cardiol,* vol. 87, pp. 178-182, 2001.

[79] M. Costa, I. Cygankiewicz, W. Zareba, A. B. d. Luna, A. L. Goldberger, and S. Lobodzinski, "Multiscale complexity analysis of heart rate dynamics in heart failure: preliminary findings from the MUSIC study," *Computers in Cardiology,* vol. 33, pp. 101-103, 2006.

[80] S. Guzzetti, M. T. L. Rovere, G. D. Pinna, R. Maestri, E. Borroni, A. Porta, A. Mortara, and A. Malliani, "Different spectral components of 24 h heart rate variability are related to different modes of death in chronic heart failure," *Eur Heart J,* vol. 26, pp. 357-362, February 2, 2005 2005.

[81] M. T. La Rovere, G. D. Pinna, R. Maestri, A. Mortara, S. Capomolla, O. Febo, R. Ferrari, M. Franchini, M. Gnemmi, C. Opaschi, P. G. Riccardi, E. Traversi, and F. Cobelli, "Short-term heart rate variability strongly predicts sudden cardiac death in chronic heart failure patients," *Circulation,* vol. 107, pp. 565-570, 2003.

[82] P. D. Welch, "The Use of Fast Fourier Transform for the Estimation of Power Spectra: A Method Based on Time Averaging Over Short, Modified Periodograms," *IEEE Transactions on Audio and Electroacoustics,* vol. AU-15, pp. 70-73, 1967.

[83] A. V. Oppenheim and R. S. Schafer, *Discrete-Time Signal Processing*, 2 ed. Englewood Cliffs: Prentice-Hall, 1999.

[84] S. M. Pincus, "Approximate entropy as a measure of system complexity," *Proc Natl Acad Sci USA,* vol. 88, pp. 2297-2301, 1991.

[85] J. S. Richman and R. Moorman, "Physiological time-series analysis using approximate entropy and sample entropy," *Am J Physiol Heart Circ Physiol,* vol. 278, pp. H2039-H2049, 2000.

[86] S. M. Pincus and A. L. Goldberger, "Physiological time-series analysis: what does regularity quantify?," *Am J Physiol,* vol. 266, pp. H1643-H1656, 1994.

[87] C.-K. Peng, S. V. Buldyrev, S. Havlin, M. Simons, H. E. Stanley, and A. L. Goldberger, "Mosaic organization of DNA nucleotides," *Physical Review E,* vol. 49, pp. 1685-1689, 1994.

[88] J. W. Kantelhardt, S. A. Zschiegner, E. Koscielny-Bunde, and A. Bunde, "Multifractal detrended fluctuation analysis of nonstationary time series," *Physica A,* vol. 316, pp. 87-114, 2002.

[89] C.-K. Peng, S. Havlin, H. E. Stanley, and A. L. Goldberger, "Quantification of scaling exponents and crossover phenomena in nonstationary heartbeat time series," *Chaos,* vol. 5, pp. 82-87, 1995.

[90] D. Fradkin and I. Muchnik, "Support Vector Machines for Classification," in *DIMACS Series in Discrete Mathematics and Theoretical Computer Science.* vol. 70, J. Abello and G. Carmode, Eds., 2006, pp. 13-20.

[91] C. Cortes and V. Vapnik, "Support-vector networks," *Machine Learning,* vol. 20, pp. 273-297, 1995.

[92] S. R. Gunn, "Support Vector Machines for Classification and Regression," Dept. of Electronics and Computer Science, University of Southampton 1998.

[93] F. E. Harrell, *Regression Modeling Strategies: With Applications to Linear Models, Logistic Regression, and Survival Analysis.* New York: Springer-Verlag, 2001.

[94] E. Vittinghoff, D. V. Glidden, S. C. Shiboski, and C. E. McCulloch, *Regression Methods in Biostatistics: Linear, Logistic, Survival, and Repeated Measures Models.* New York: Springer-Verlag, 2005.

[95] D. R. Cox, "Regression models and life-tables," *Journal of the Royal Statistical Society. Series B.,* vol. 34, pp. 187-220, 1972.

[96] H. Motulsky, *Intuitive Biostatistics.* New York: Oxford University Press, Inc., 2995.

[97] G.-Q. Wu, N. M. Arzeno, L.-L. Shen, D.-K. Tang, D.-A. Zheng, N.-Q. Zhao, D. L. Eckberg, and C.-S. Poon, "Chaotic signatures of heart rate variability in health, aging, and heart failure," 2007.

[98] J. A. Taylor, D. L. Carr, C. W. Myers, and D. L. Eckberg, "Mechanisms underlying very-low-frequency RR-interval oscillations in humans," *Circulation,* vol. 98, pp. 547-555, 1998.